Microstructure evolution during recrystallization of dual-phase steels

D. Raabe, F. Roters, D. Ponge, S. Zaefferer, N. Perannio, M. Calcagnotto

Max-Planck-Institut
für Eisenforschung GmbH
Düsseldorf, Germany

WWW.MPIE.DE
d.raabe@mpie.de

RX&GG 4, July 2010, Sheffield

Overview

- Motivation
- Experiments
- Microstructure and texture evolution
- 3D tomographic analysis of interface regions
- Correlation to DP mechanical properties
- Ultra-fine grained DP
- Conclusions

Raabe: Adv. Mater. 14 (2002), Roters et al. Acta Materi.58 (2010)

Overview

- Low energy consumption through weight reduction: high-strength steels with a good formability such as C Mn DP
- Microstructure evolution in hot rolled, cold rolled, and hot-dip galvanized dual-phase steel sheets
- Dominating mechanisms during intercritical annealing: recovery, recrystallization, phase transformation and competition between them
- Important role of annealing parameters such as heating rate, intercritical annealing temperature, annealing time, cooling rate, and the final annealing temperature
- Through-thickness inhomogeneity: introduced by hot and cold rolling, leading to a plane-strain texture in the center layer and a shear texture close to the surface of the sheets
- Microstructure and texture evolution in DP steels considering through-thickness inhomogeneity
- Spatial distribution of the DP constituents through-thickness
- Annealing experiments in a wide temperature and time range

Overview

- Motivation
- Experiments
- Microstructure and texture evolution
- 3D tomographic analysis of interface regions
- Correlation to DP mechanical properties
- Ultra-fine grained DP
- Conclusions

Calcagnotto et al. Mater. Sc. Engin. A 527 (2010) 2738

Chemical composition of hot band in wt. %.

Fe	C	Si	Mn	P	S	N	Al	Cu
bal.	0.147	0.403	1.868	0.01	0.002	0.0056	0.037	0.028
Cr	**Ni**	**V**	**Ti**	**Nb**	**Mo**	**Sn**	**B**	
0.028	0.044	0.098	0.005	0.047	0.003	0.009	0.0001	

Hot rolled to 3.75 mm as starting material

Volume fractions of 65% ferrite and 35% pearlite

Cold rolled to thicknesses of 2.2 mm, 1.75 mm, and 1.5 mm

Experiments

- hot rolled (3.5 mm, 70% ferrite, 30% pearlite, 0.147 wt% C, 1.9 wt. % Mn, 0.4 wt.% Al)
- cold rolled in laboratory (1.70 mm, 50%)
- industrially cold rolled (2.2 mm, 1.75 mm, 1.5 mm, 63%, 50%, 43%)
- annealing of industrially cold rolled (1.75 mm, 50%) sheets
  - salt bath (MPIE) / conductive annealing (SZMF)
  - annealing temperature 740°C≈Ac_1, 860°C≈Ac_3, and 920°C
  - annealing time 100 s, 200 s, and 300 s
  - cooling rate 7 K/s, 15 K/s, and 22 K/s
  - heating rate 10 K/s, 20 K/s, and 30 K/s

Intercritical deformation and isothermal holding

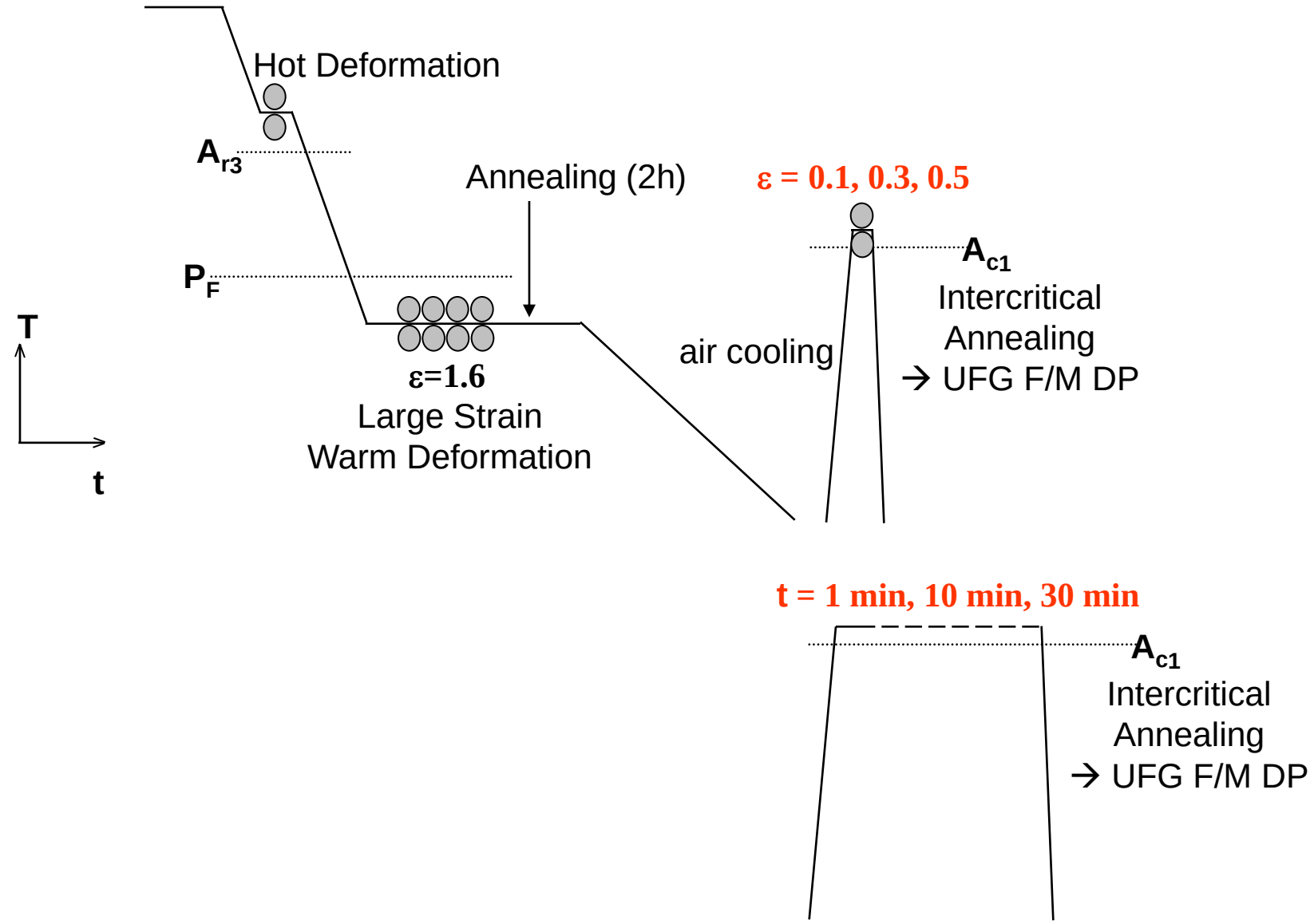

phase changes in dual phase steels

cold rolled

intercritical annealing

room temperature

deformed ferrite

pearlite

recrystallized ferrite

recovered ferrite

strain free austenite

recrystallized/ strain free ferrite

recovered/strained ferrite

martensite

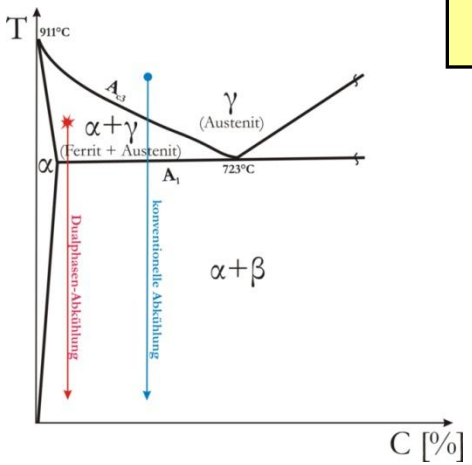

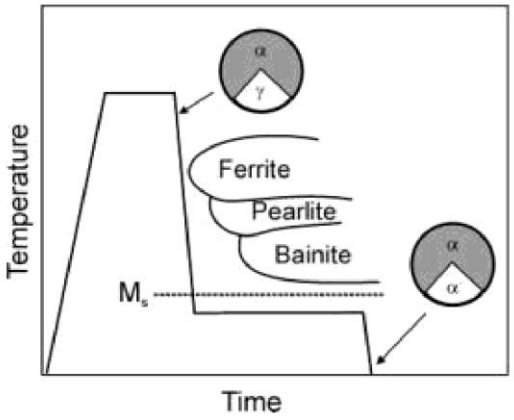

Overview

- Motivation
- Experiments
- Microstructure and texture evolution
- 3D tomographic analysis of interface regions
- Correlation to DP mechanical properties
- Ultra-fine grained DP
- Conclusions

Raabe: Adv. Mater. 14 (2002), Roters et al. Acta Materi.58 (2010)

Microstructure evolution

hot rolled, thickness 3.75 mm	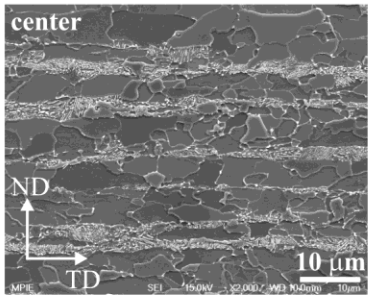	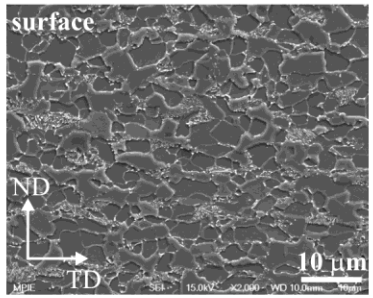
cold rolled, thickness 1.75 mm	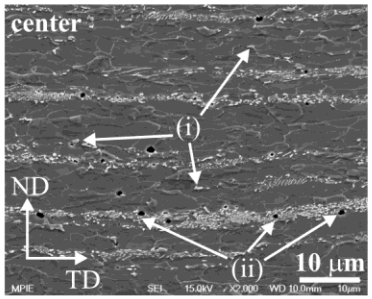	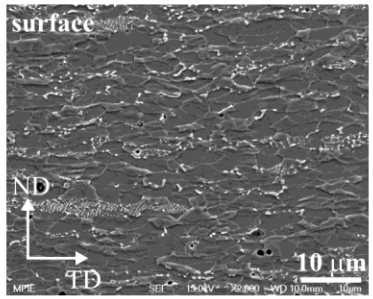
hot-dip galvanized at 830°C for 80s	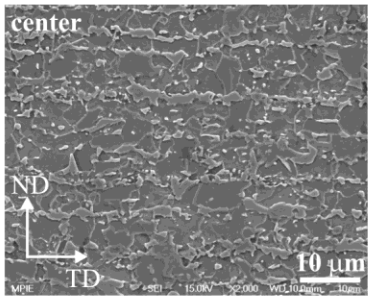	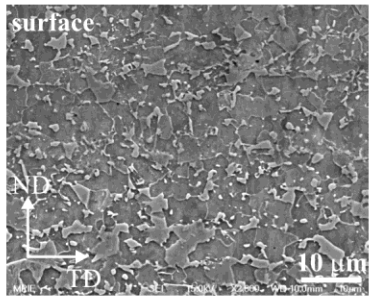
conductively annealed at 920°C for 100 s, heating rate 20 K/s, cooling rate -15 K/s	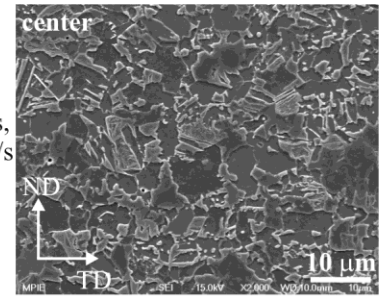	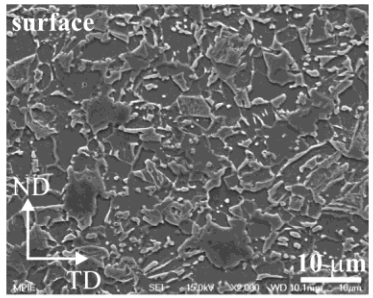

Microstructure and texture evolution – hot band through thickness

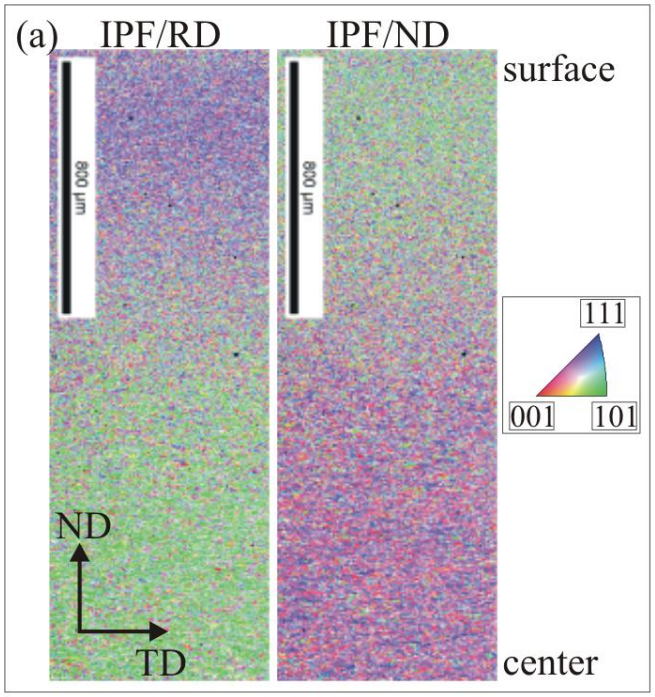

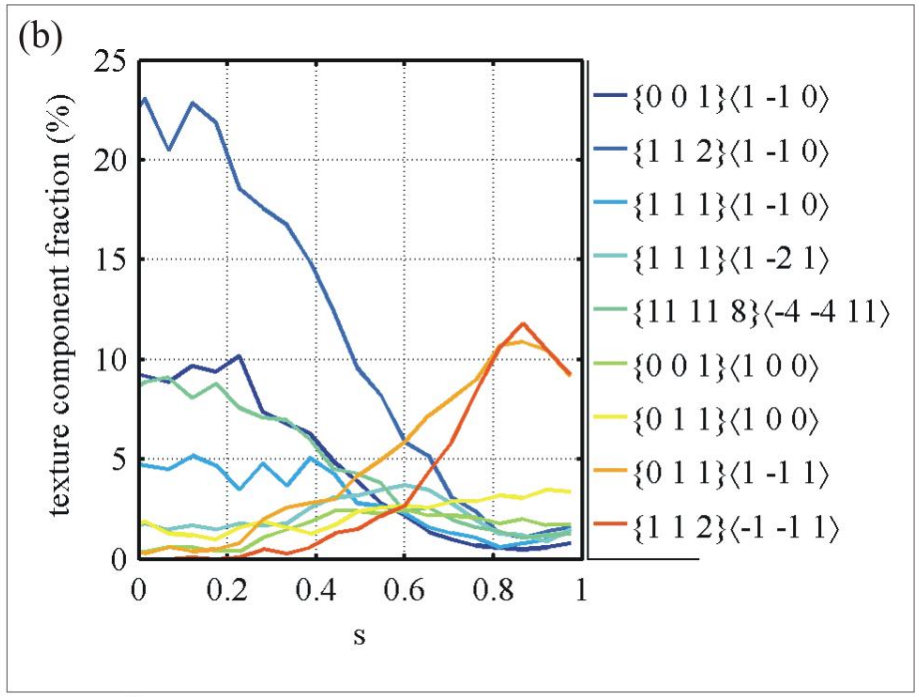

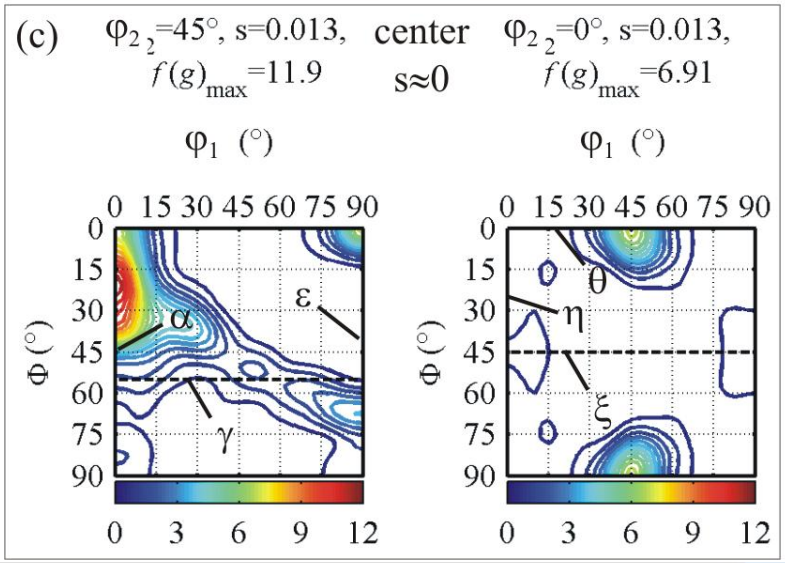

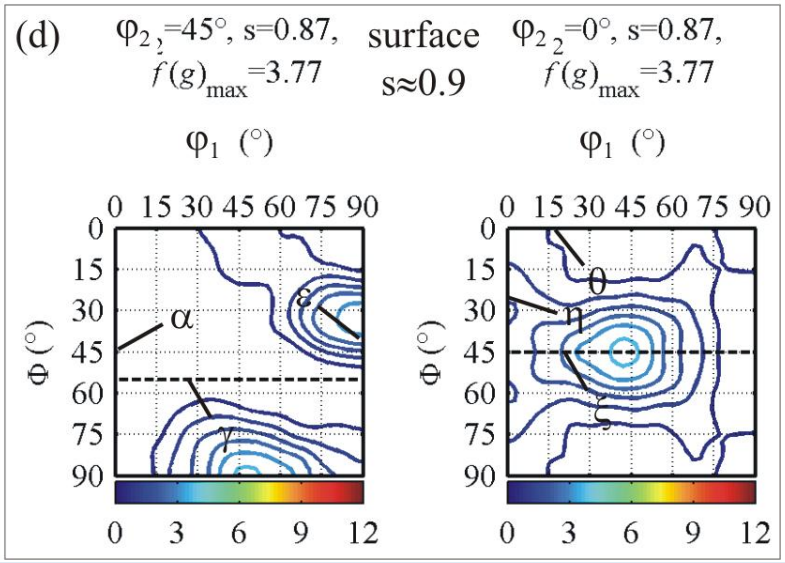

Texture evolution –rolled, annealed, through thickness

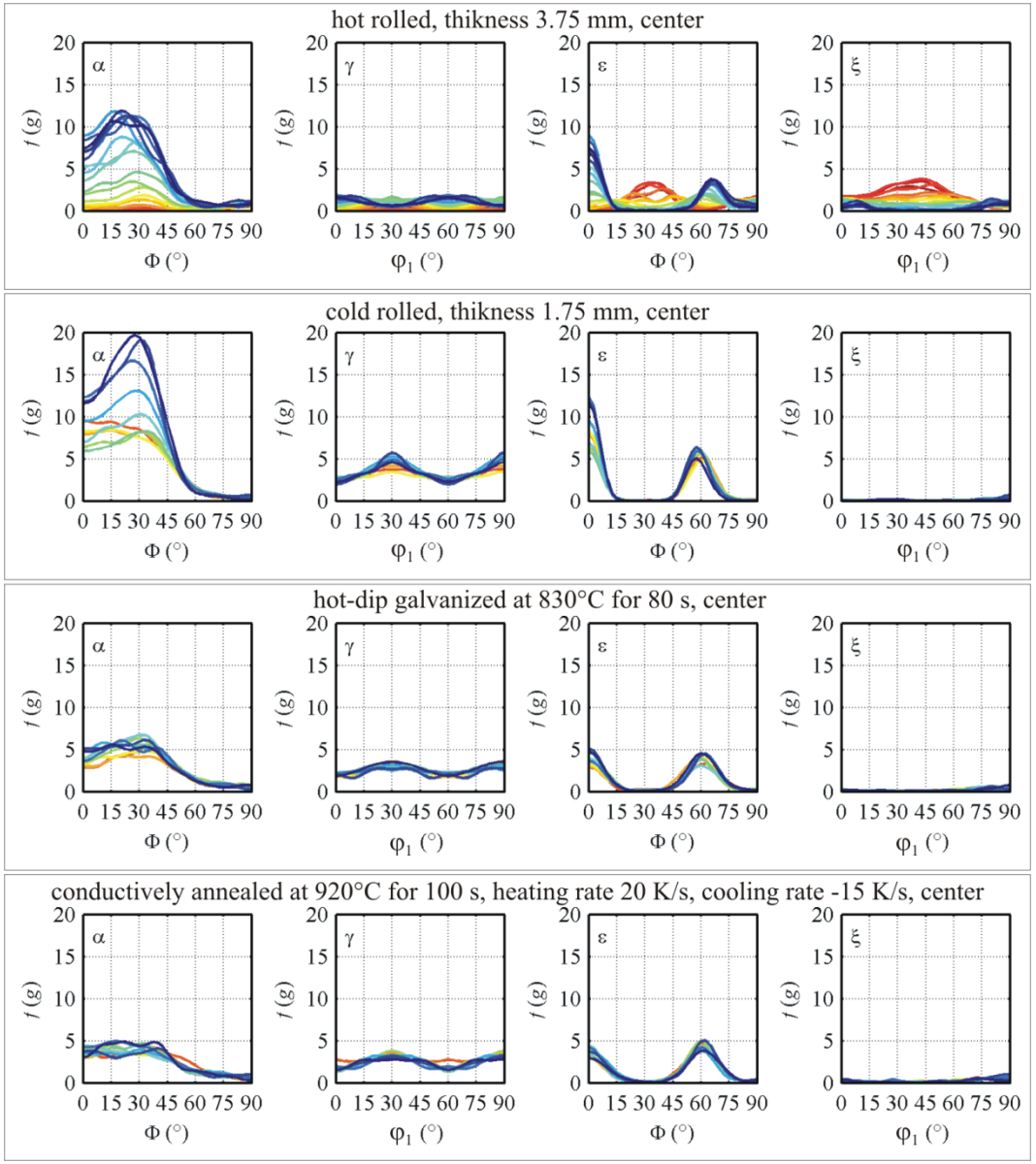

Texture and microstructure–rolled, annealed, through thickness

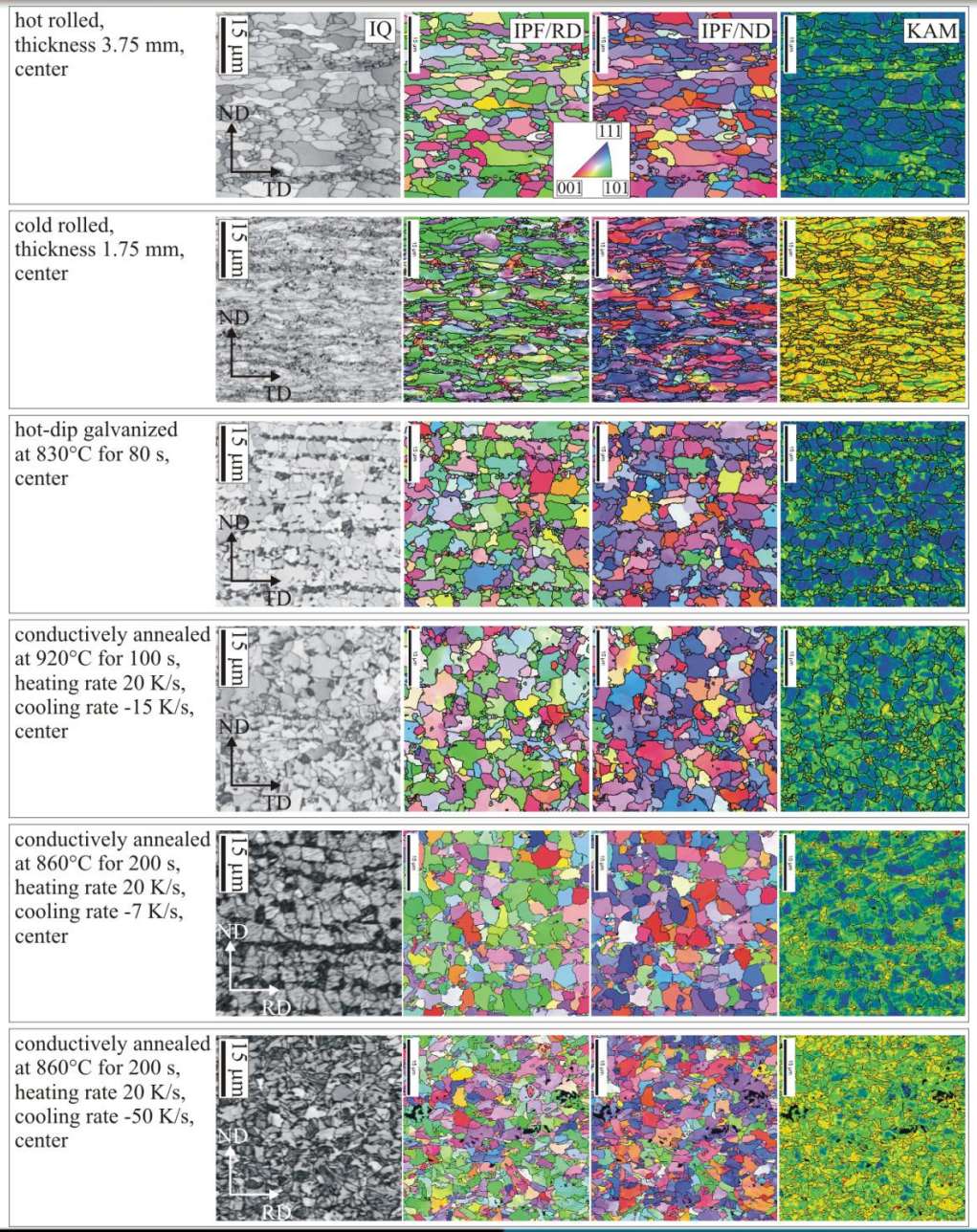

Results - EBSD – cold rolled

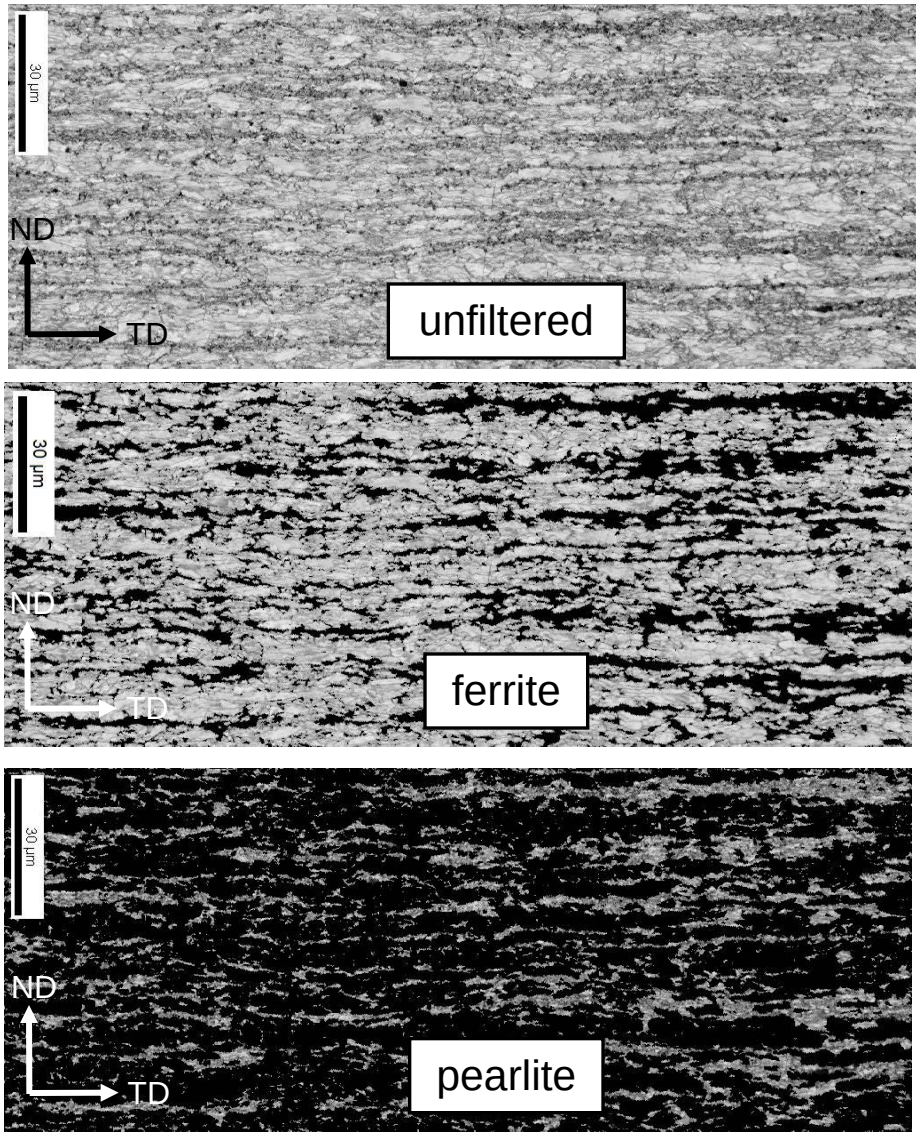

cold rolled, center of sample

- image quality signal allows separate analysis of the constituents
- ferrite volume fraction 74%
- grain size 4.8 µm, aspect ratio 0.26
- large grains are deformed

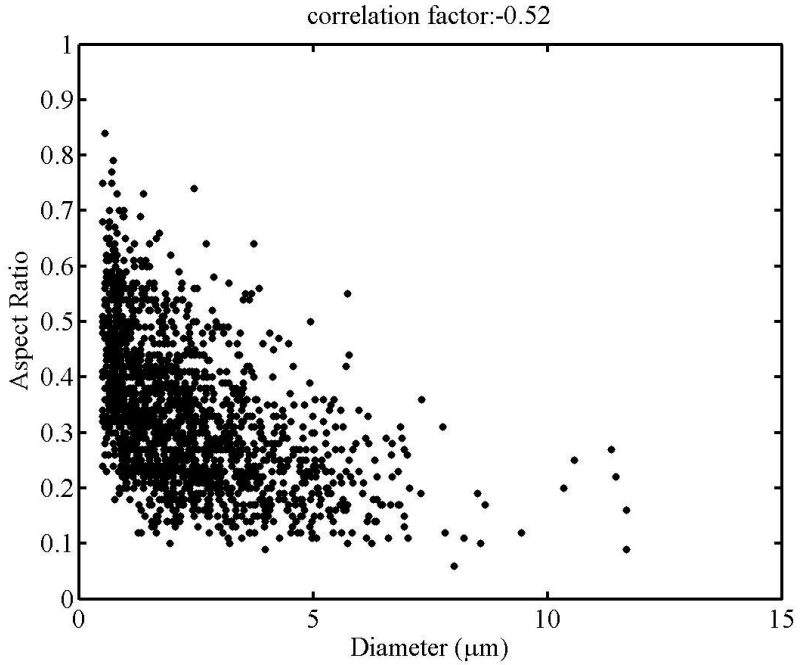

Results - EBSD – cold rolled

inverse pole figures and ODF, cold rolled, center

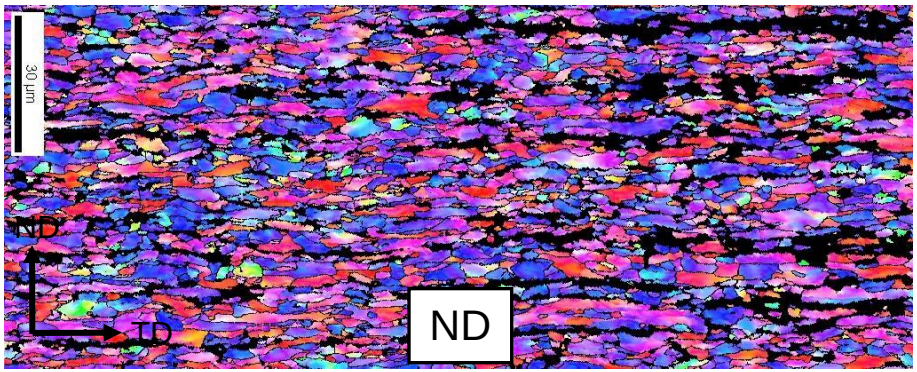

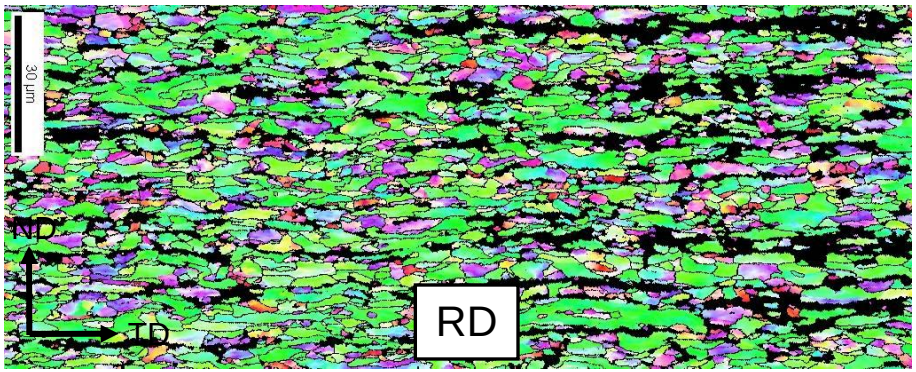

- <110> parallel RD (α-fiber), {111} parallel ND (γ-fiber)
- typical texture for bcc-materials

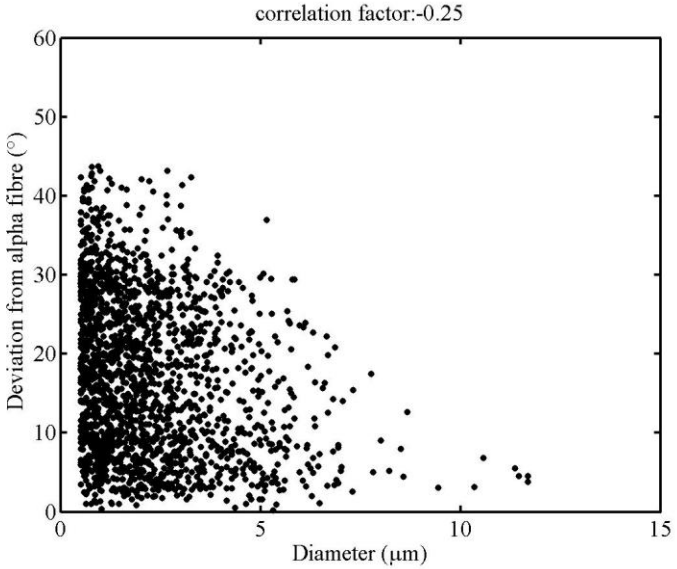

large grains are closer to the α-fiber

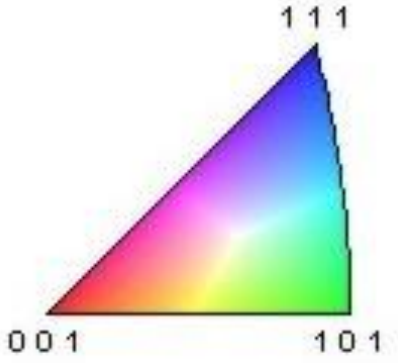

Competition: recrystallization -transformation, through thickness

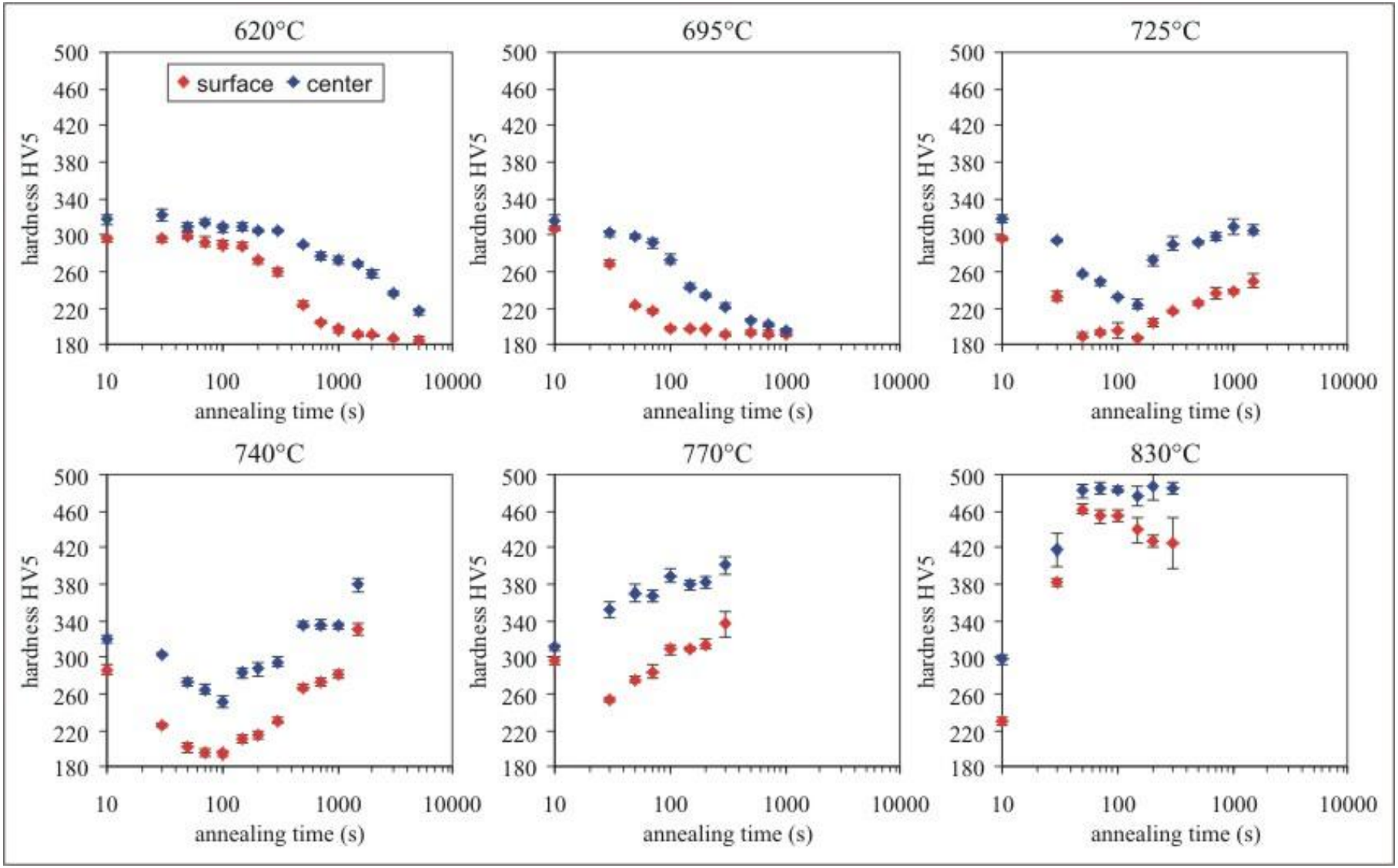

Competition: recrystallization -transformation, through thickness

annealed in
salt bath at
740°C for 100 s

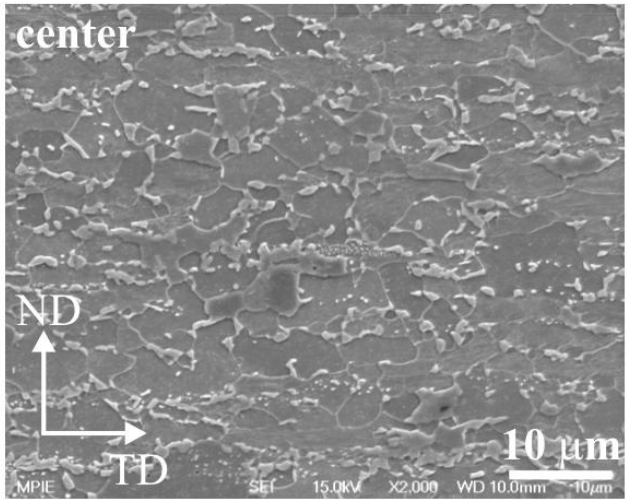

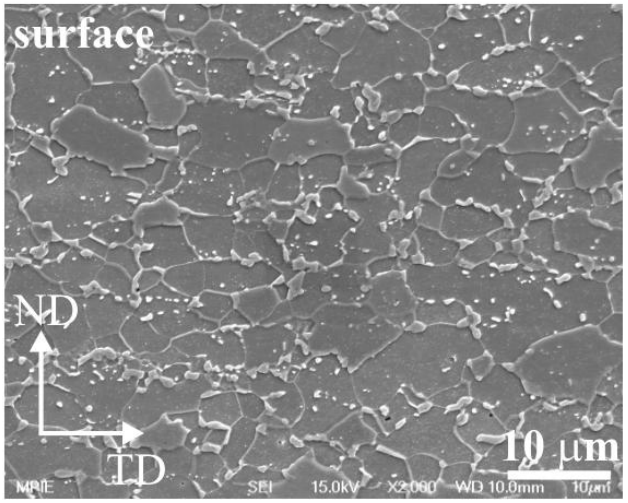

conductively
annealed at
740°C for 100 s,
heating rate 20 K/s,
cooling rate -15 K/s

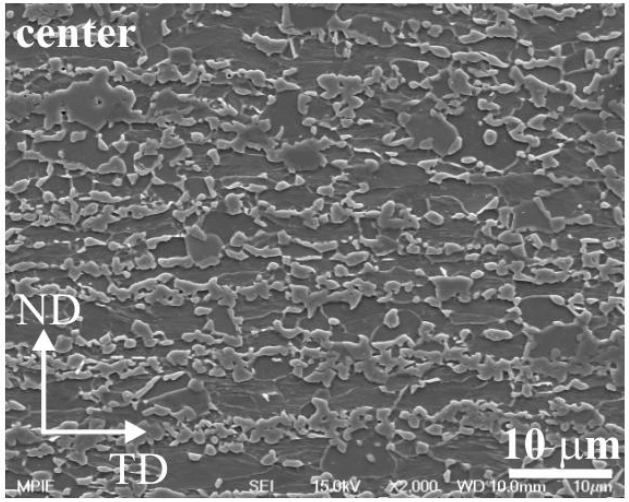

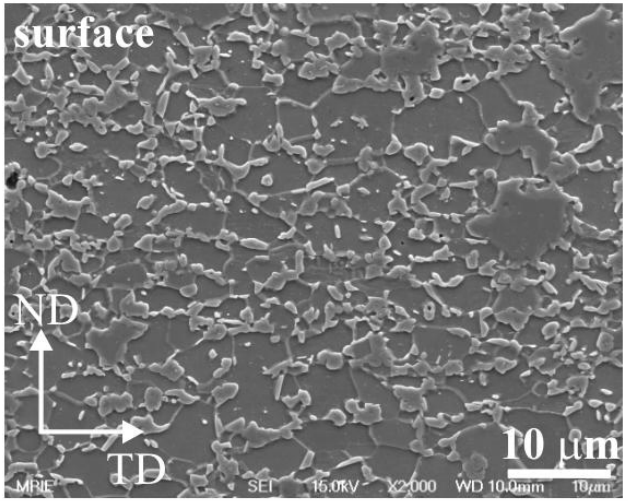

Competition: recrystallization -transformation, through thickness

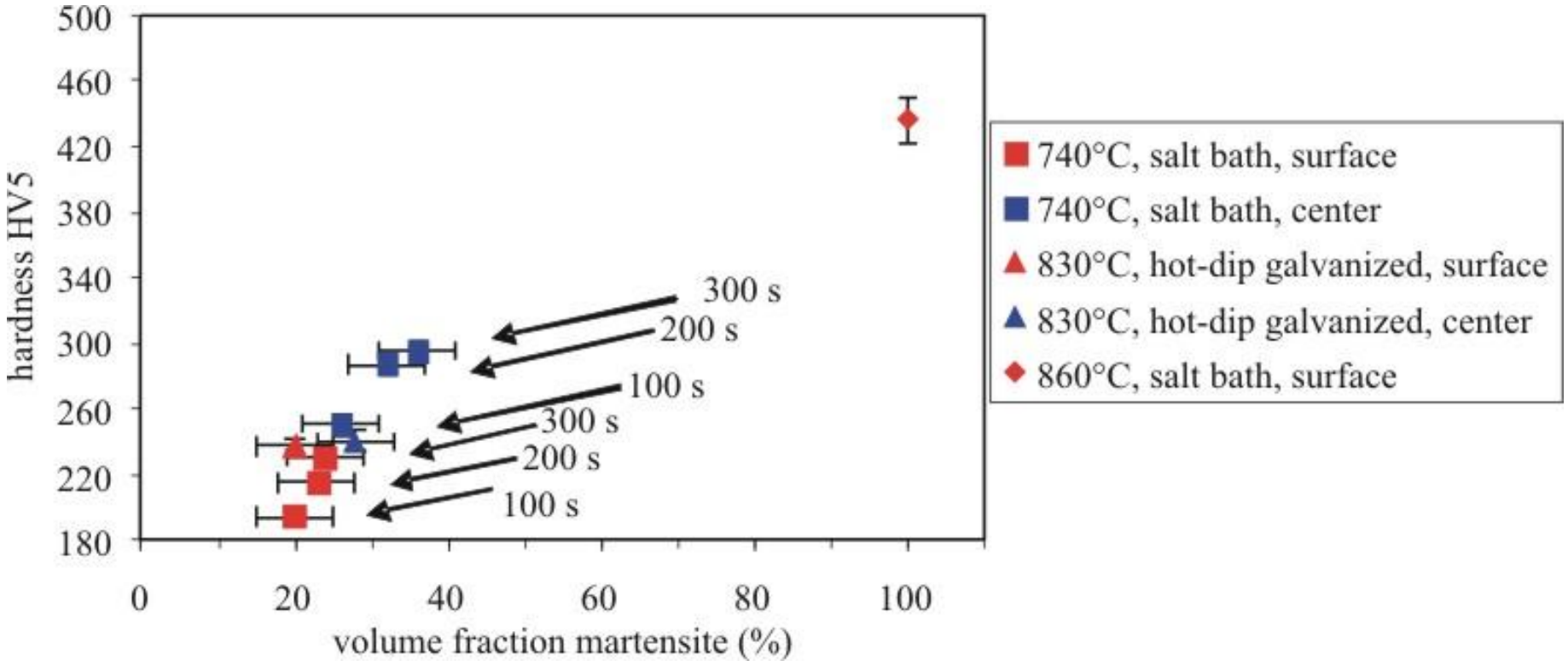

Calcagnotto et al. Mater. Sc. Engin. A 527 (2010) 2738

Texture: recrystallization -transformation, through thickness

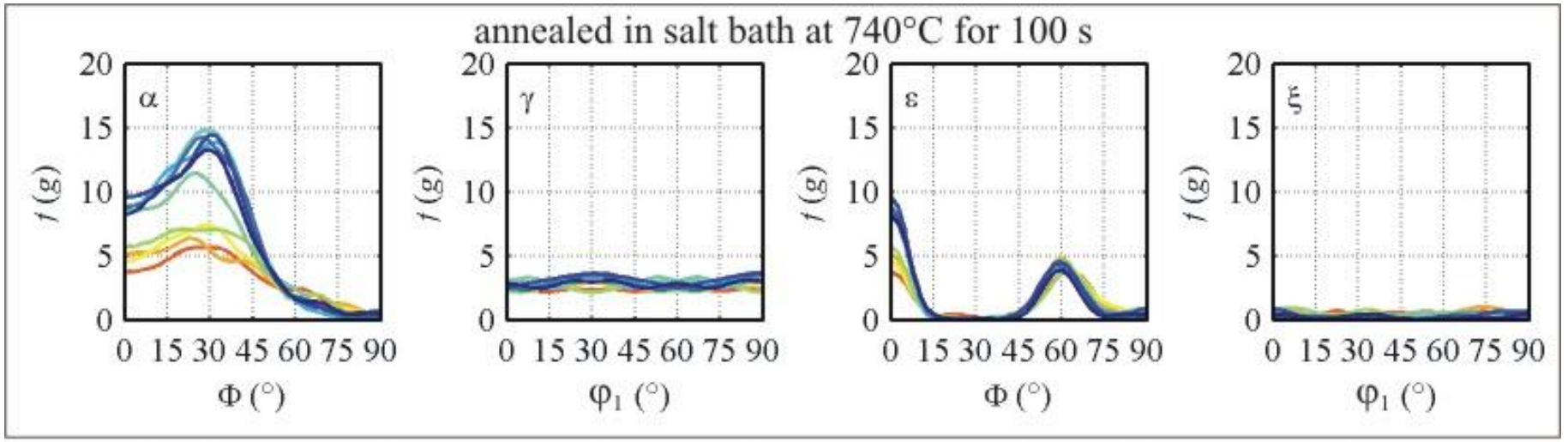

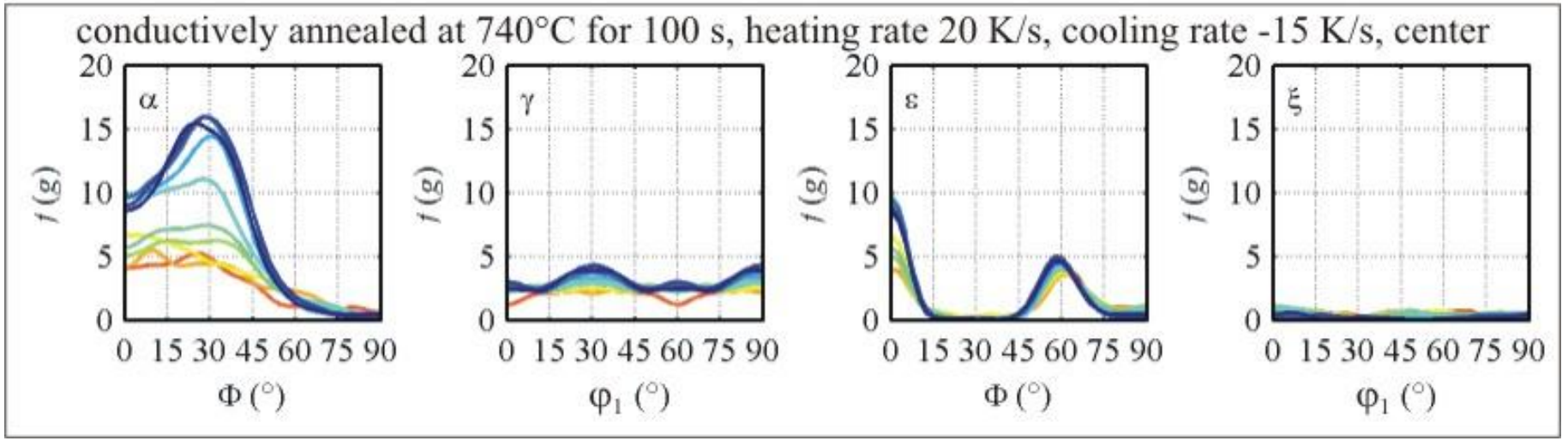

Overview

- Motivation
- Experiments
- Microstructure and texture evolution
- 3D tomographic analysis of interface regions
- Correlation to DP mechanical properties
- Ultra-fine grained DP
- Conclusions

Raabe: Adv. Mater. 14 (2002), Roters et al. Acta Materi.58 (2010)

3D EBSD: joint FIB-EBSD tomography

- Increase phase space of microstructure analysis
  6D (φ_1,ϕ,φ_2,x,y,z): Crystallography and texture with morphology
  8D (φ_1,ϕ,φ_2,h,k,x,y,z): Interface crystallography (interface texture)

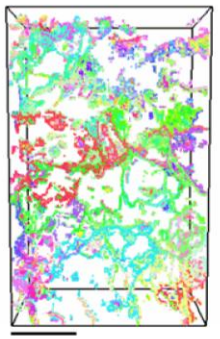

- Spatial texture and phases (connectivity, percolation, correlations)

- Sectioning by FIB
  accurate depth definition, flat parallel sections, high resolution (< 50 nm)
- Observation by EBSD
  good contrast on crystalline material, reconstruction in 2D and 3D, quantitative, high resolution (~ 50 nm),
- Combination of FIB and EBSD
  high measurement speed, fully automatic

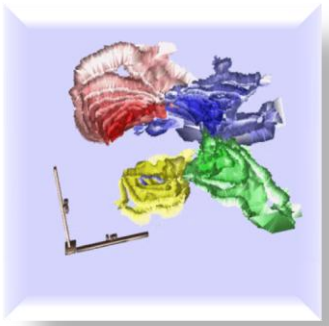

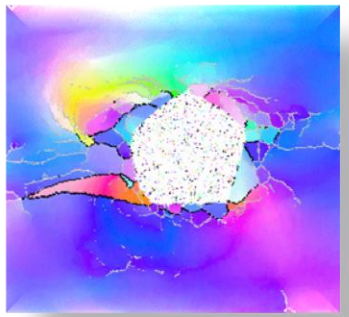

Recent review:
- *Zaefferer et al., Met. Mater. Trans. 39A, (2008) 374*

Konrad et al. Acta Mater. 54 (2006) 1369

Instrument overview

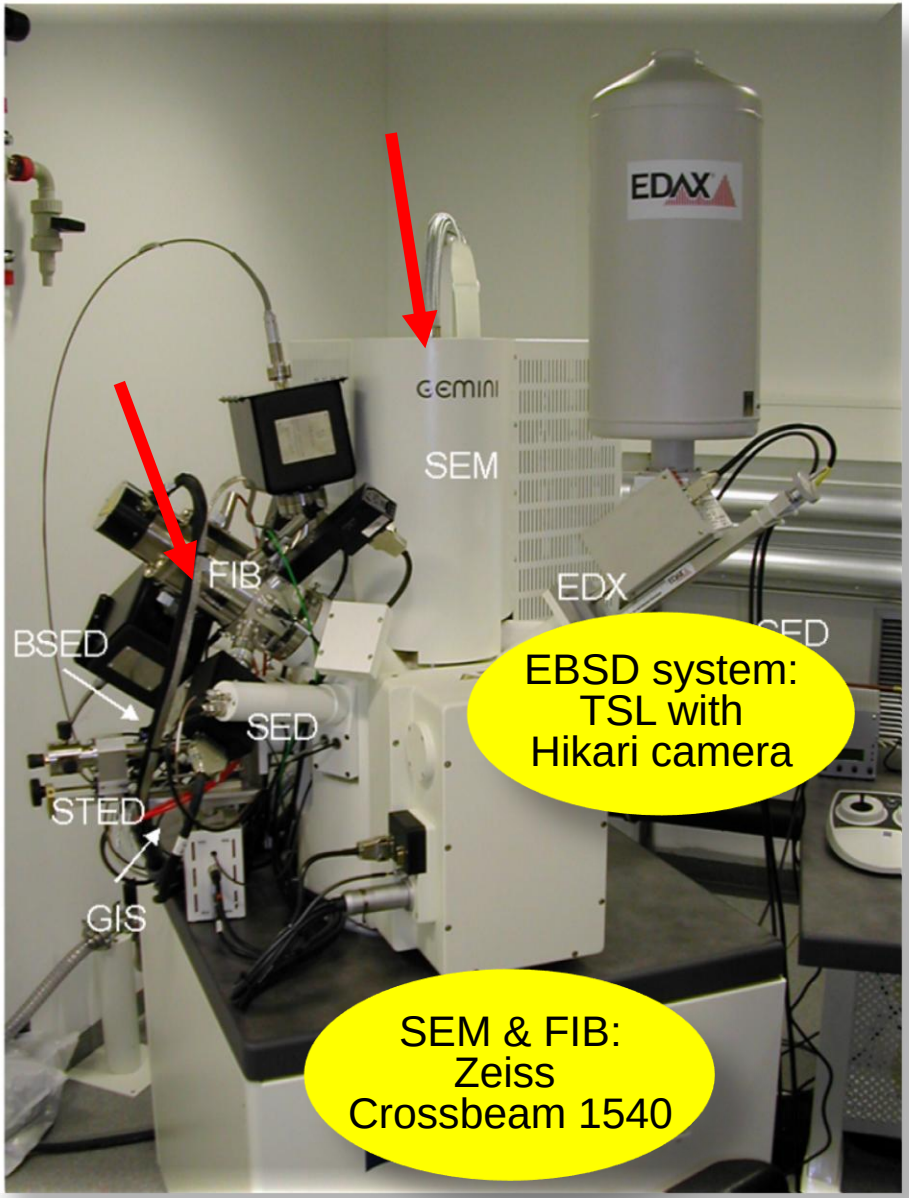

- Scanning electron microscope (SEM)
  - observation of microstructure
- Scanning Ga^+-ion microscope (FIB = focused ion beam)
  - sputtering of material for serial sectioning
- Quantitative images with EBSD and EDX
  - quantitative characterisation of microstructure

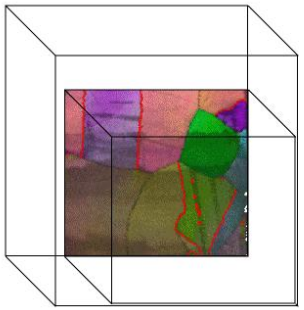

Zaefferer et al., Met. Mater. Trans. 39A (2008) 374

Principle of serial sectioning & orientation microscopy

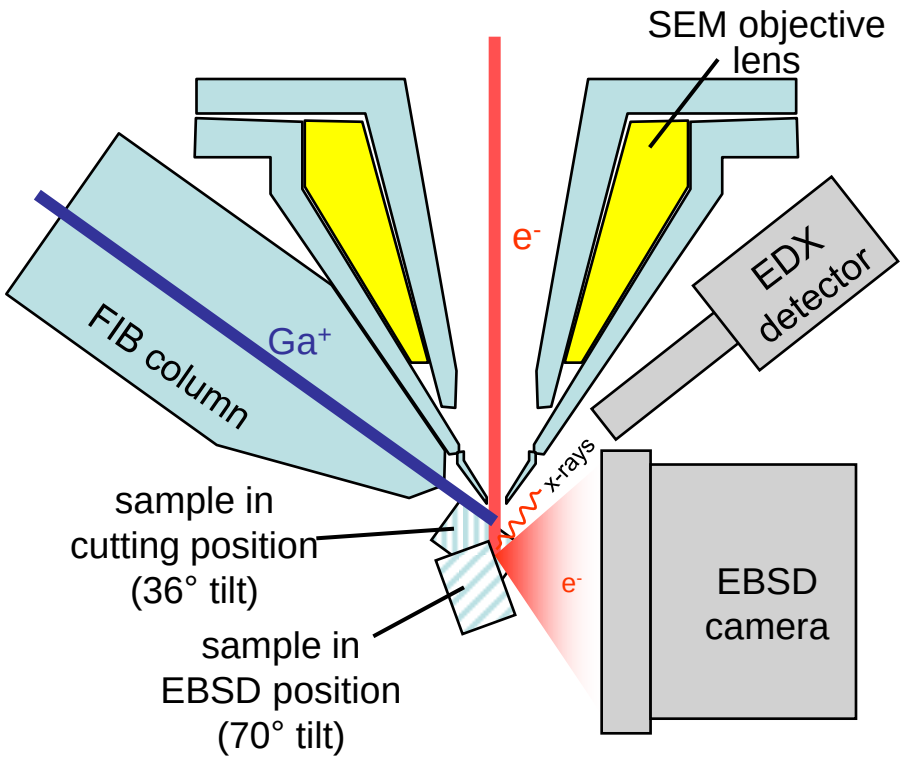

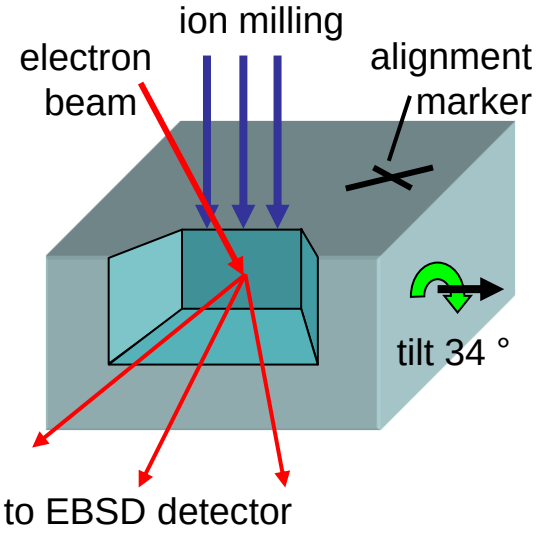

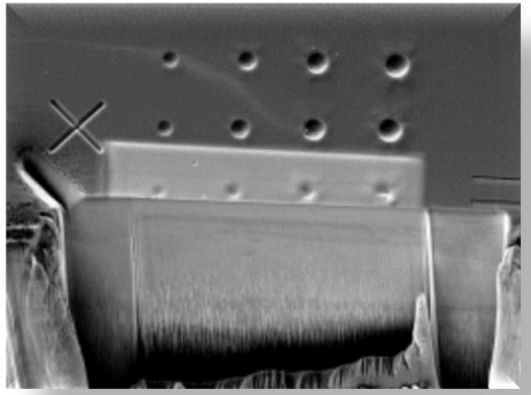

Approaches to 8D interface analysis and 3D GND analysis

Plane boundaries defined by triple junctions in two adjacent layers

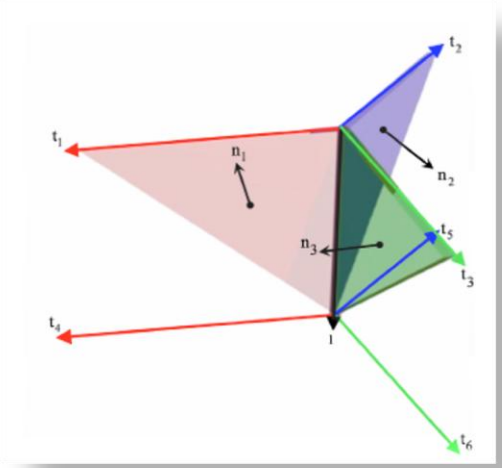

Greg Rohrer

Triangulation the interfaces for defining the grain boundaries

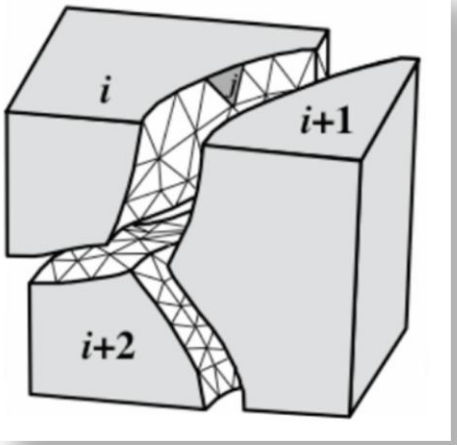

Tony Rollett

GND (Kröner-Nye)

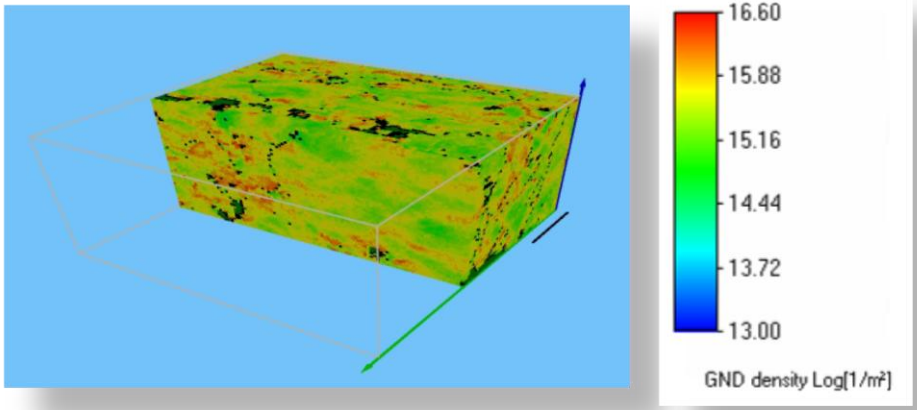

From local misorientations to GNDs

$$\triangle\phi = \phi_{(2)}\ \phi_{(1)}^{-1}$$ misorientation

$$|\triangle\phi| = min\{cos^{-1}\{tr[(O_i^{cry}\phi_{(1)})\phi_{(2)}^T O_j^{cry}]\}\} \quad i = 1\ldots24,\ j = 1\ldots24$$

$$\phi_{(2)} - \phi_{(1)} = (\triangle\phi - I)\phi_{(1)}$$ orientation difference

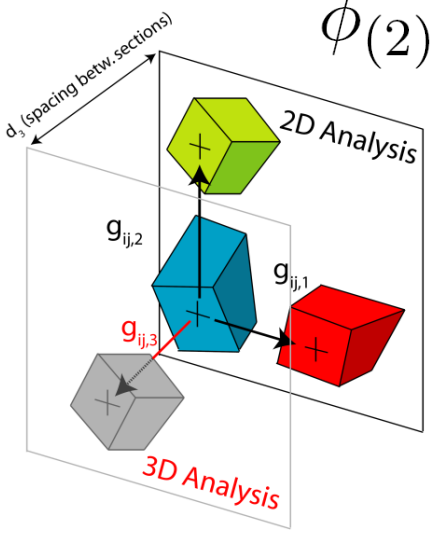

$$g_{ij,k} = \frac{\phi_{(2)ij} - \phi_{(1)ij}}{d_k}$$

orientation gradient
(spacing d from EBSD scan)

From local misorientations to GNDs

$$\beta_{ij} = \frac{\delta u_i}{\delta x_j} = \beta_{ij}^{el} + \beta_{ij}^{pl}$$

distortion
(sym, a-sym)

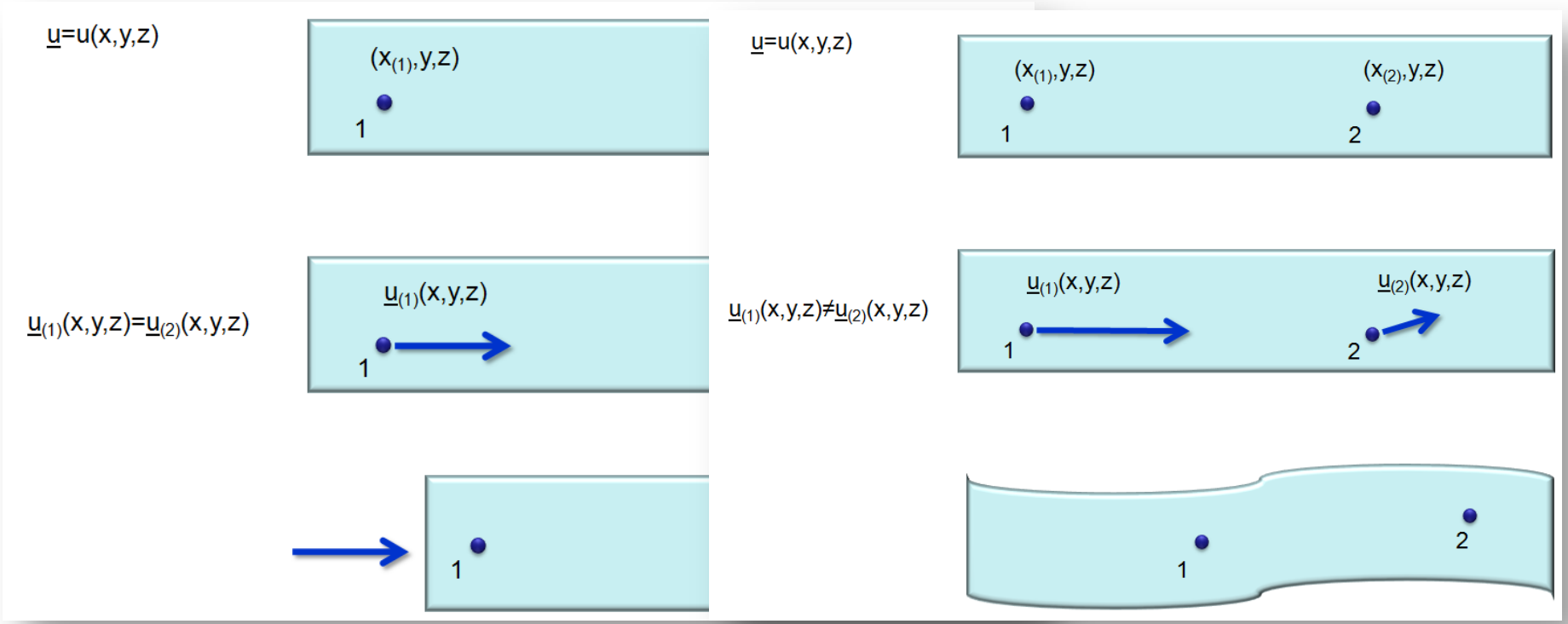

From local misorientations to GNDs

$$\beta_{ij} = \frac{\delta u_i}{\delta x_j} = \beta_{ij}^{el} + \beta_{ij}^{pl}$$

distortion
(sym, a-sym)

$$\alpha = \nabla \times \beta^{el}$$

$$\alpha_{pi} = e_{pkj} \left(\epsilon_{ij,k}^{el} + g_{ij,k} \right)$$

$$\alpha_{pi} = e_{pkj} \, g_{ij,k}$$

dislocation tensor (GND)

J. F. Nye. Some geometrical relations in dislocated crystals. Acta Metall. 1:153, 1953.
E. Kröner. Kontinuumstheorie der Versetzungen und Eigenspannungen (in German). Springer, Berlin, 1958.
E. Kröner. Physics of defects, chapter Continuum theory of defects, p.217. North-Holland Publishing, Amsterdam, Netherlands, 1981.

From local misorientations to GNDs

Slip and line directions of dislocations for GNDs in a FCC crystal

$\sqrt{2}\,\hat{\mathbf{b}}$:	$\bar{1}10$	$10\bar{1}$	$0\bar{1}1$	$\bar{1}\bar{1}0$	101	$01\bar{1}$	110	$\bar{1}01$	$0\bar{1}\bar{1}$	$1\bar{1}0$	$\bar{1}0\bar{1}$	011	110	101	011	$\bar{1}10$	$10\bar{1}$	$0\bar{1}1$
$\sqrt{6}\,\hat{\mathbf{t}}$:	$\bar{1}\bar{1}2$	$\bar{1}2\bar{1}$	$2\bar{1}\bar{1}$	$\bar{1}1\bar{2}$	$\bar{1}\bar{2}1$	211	$1\bar{1}\bar{2}$	121	$\bar{2}\bar{1}1$	112	$1\bar{2}\bar{1}$	$\bar{2}1\bar{1}$	110	101	011	$\bar{1}10$	$10\bar{1}$	$0\bar{1}1$

$$\mathbf{B} = \mathbf{b}(\hat{\mathbf{t}} \cdot \mathbf{r}) = (\mathbf{b} \otimes \hat{\mathbf{t}})\mathbf{r}$$

Frank loop thro

$$\alpha_{ij} = \sum_{a=1}^{18} \rho_{gnd}^{a}\, b_i^a t_j^a$$

18 b,t combination

$$\alpha_{ij} = \sum_{a=1}^{9} \rho_{gnd}^{a}\, b_i^a t_j^a$$

9 b,t combinations

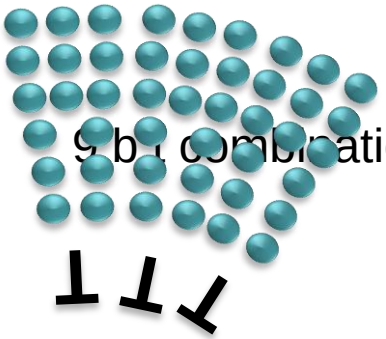

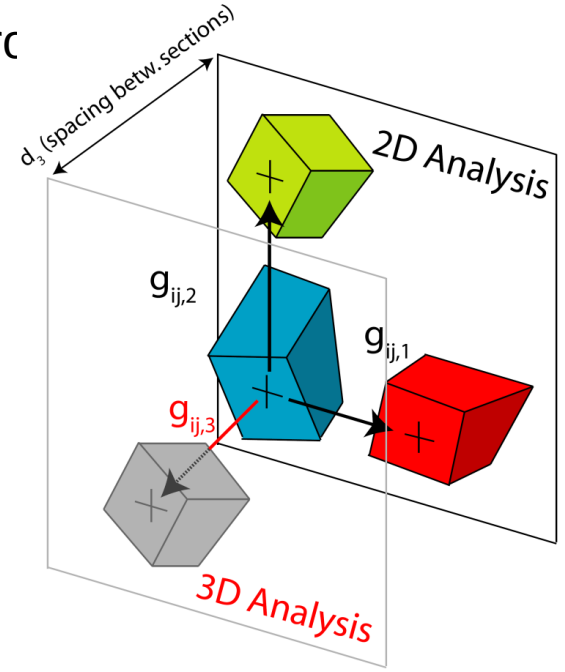

3D EBSD analysis of DP microstructure and texture

martensite

ferrite

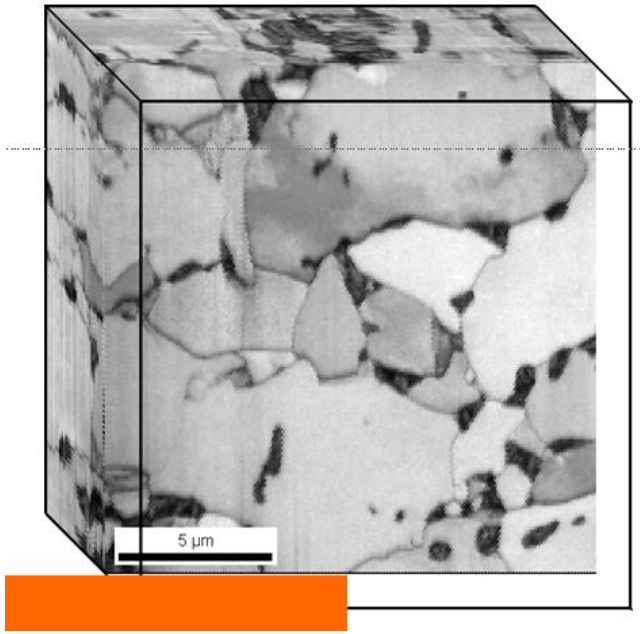

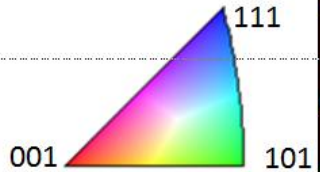

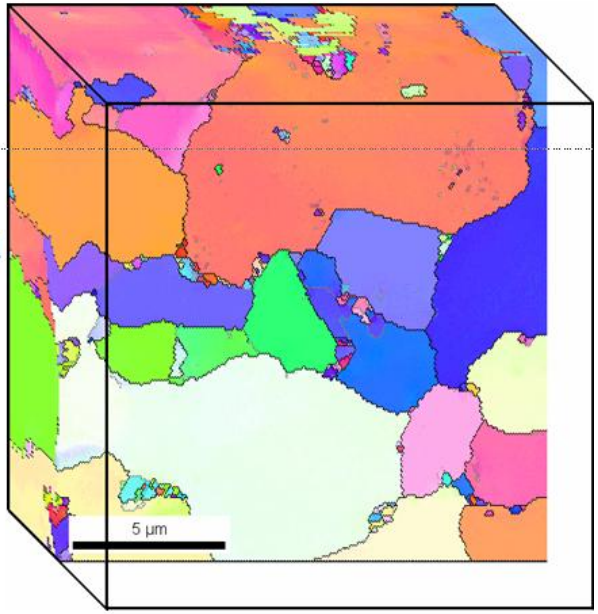

Calcagnotto et al. Mater. Sc. Engin. A 527 (2010) 2738

Overview

- Motivation
- Experiments
- Microstructure and texture evolution
- 3D tomographic analysis of interface regions
- Correlation to DP mechanical properties
- Ultra-fine grained DP
- Conclusions

3D EBSD analysis of DP microstructure and texture

Image Quality

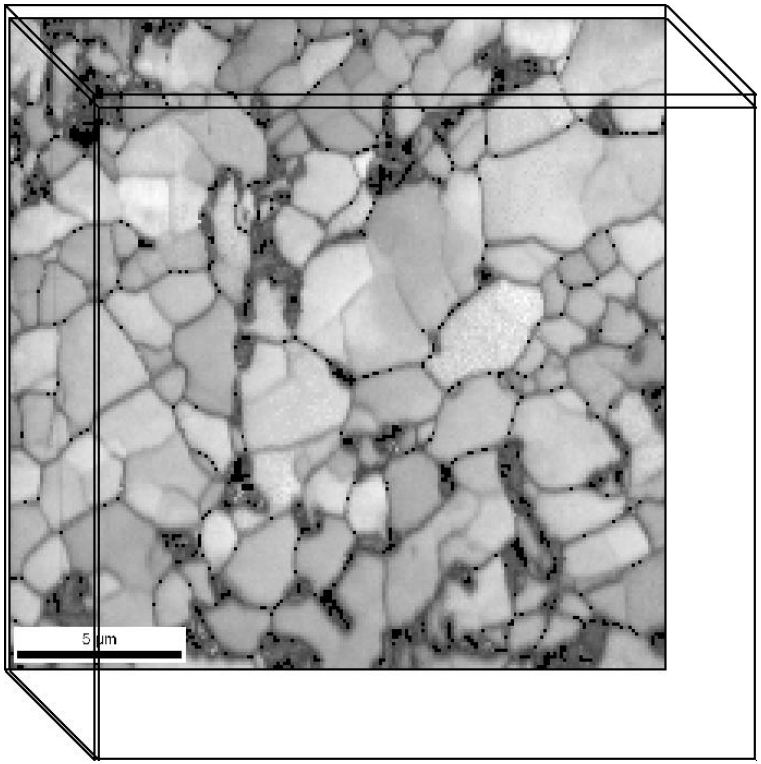

Kernel Average Misorientation
(martensite highlighted in black)

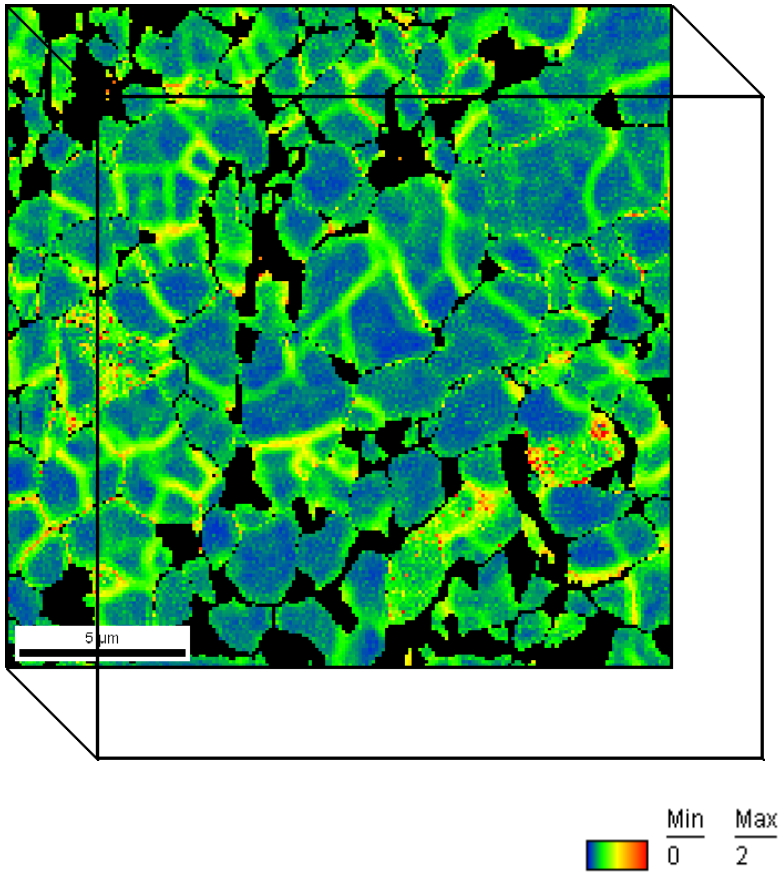

GND analysis of DP microstructure and texture

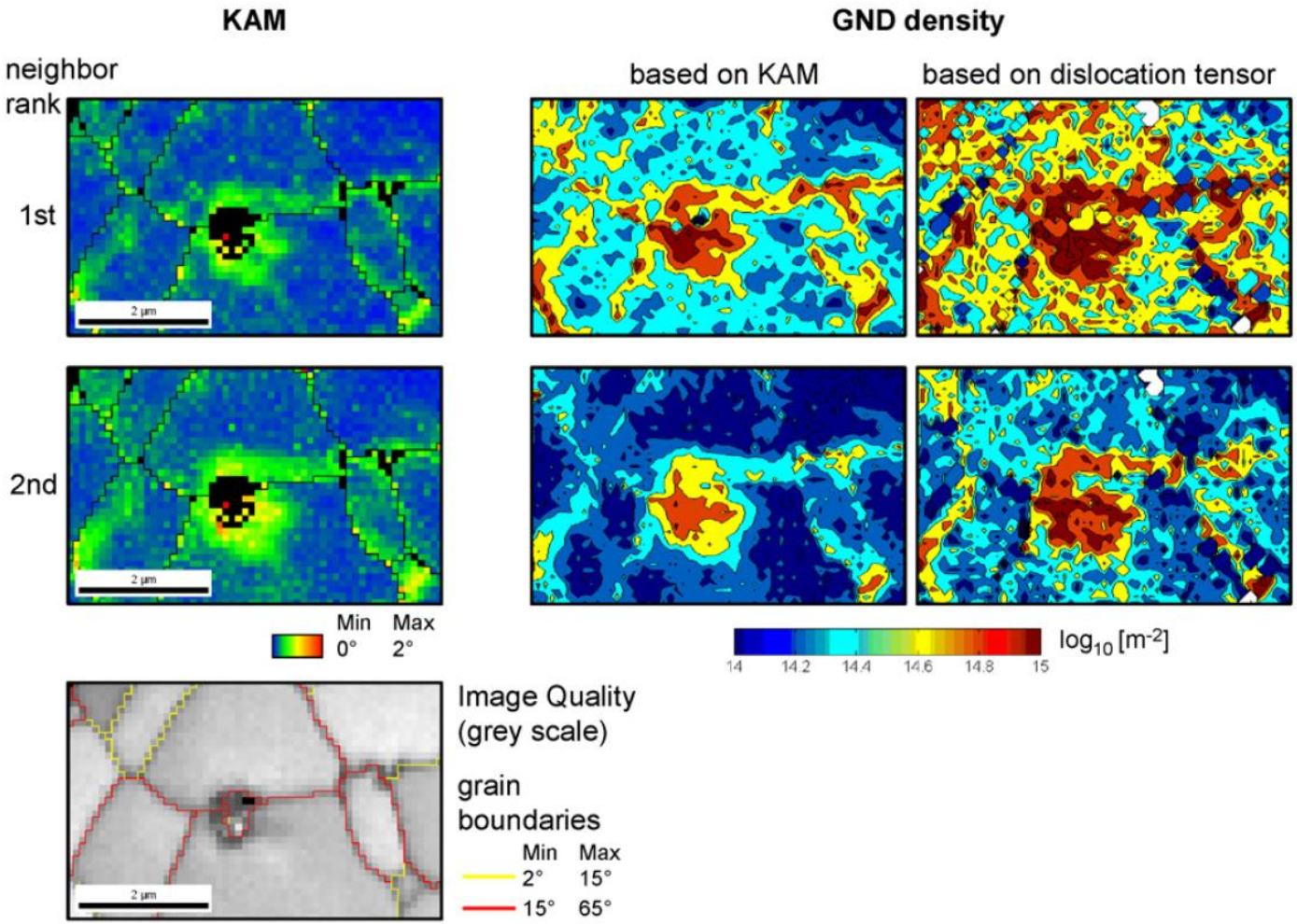

3D GND analysis of DP microstructure

misorientation FF
misorientation FM
IQ FF
IQ FM

misorientation [°]
Image Quality
distance [µm]

ferrite-martensite interfaces

ferrite-ferrite interfaces

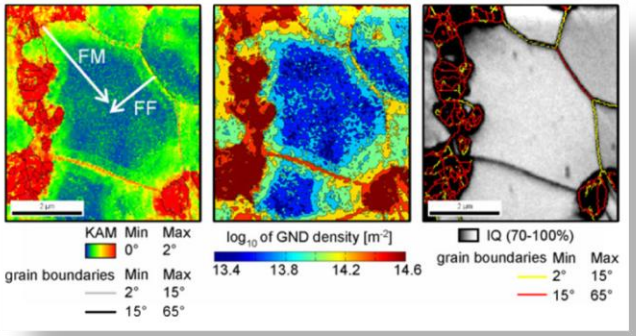

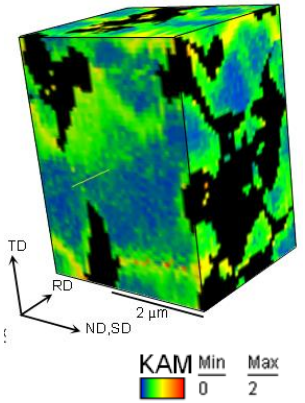

Calcagnotto et al. Mater. Sc. Engin. A 527 (2010) 2738

Overview

- Motivation
- Experiments
- Microstructure and texture evolution
- 3D tomographic analysis of interface regions
- Correlation to DP mechanical properties
- Ultra-fine grained DP
- Conclusions

Raabe: Adv. Mater. 14 (2002), Roters et al. Acta Materi.58 (2010)

Ultrafine grained DP steels

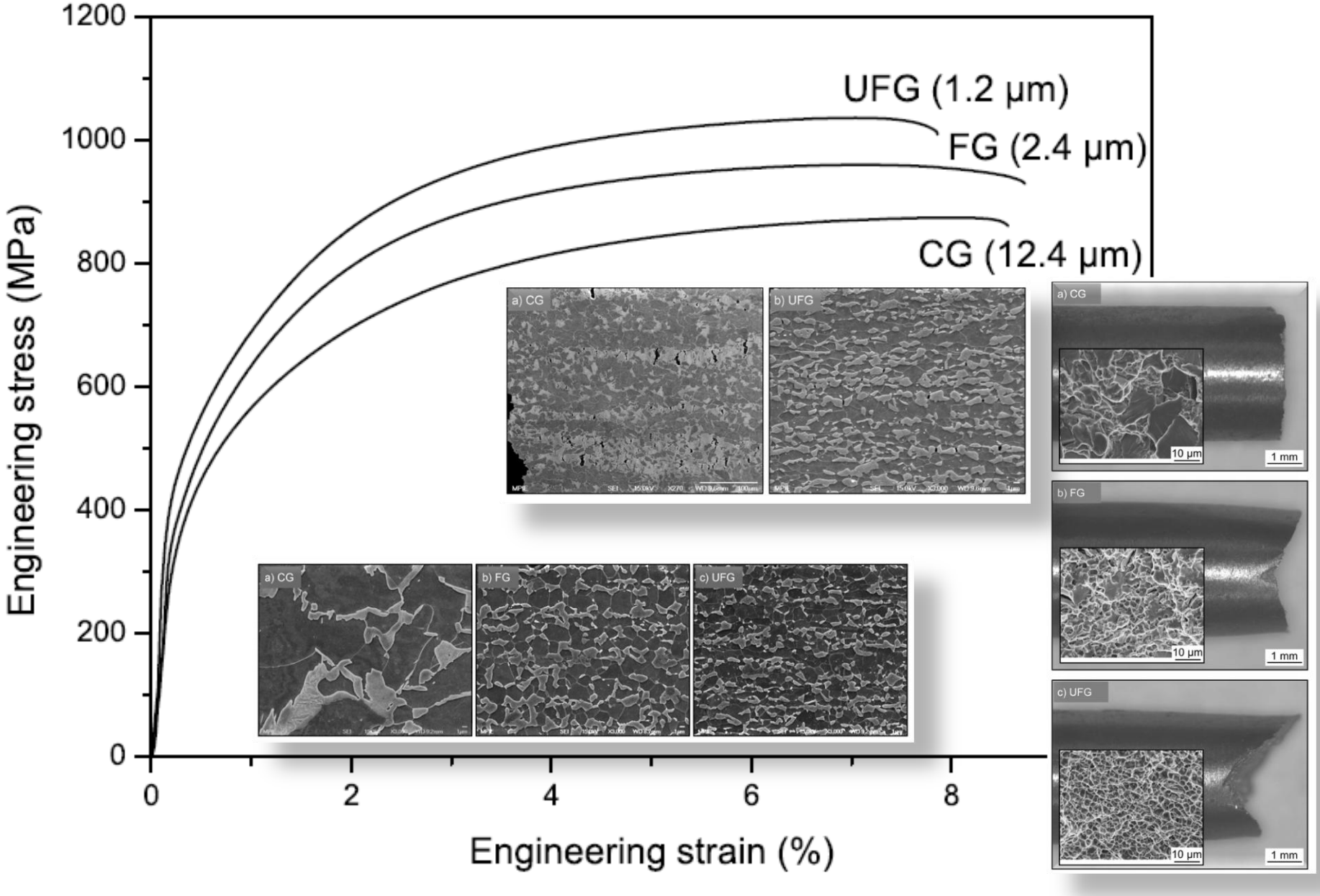

Calcagnotto et al. Mater. Sc. Engin. A 527 (2010) 2738

3D GND analysis of DP microstructure

Coarse grained DP (12.4 µm)

Berkovich 50 nm
Constant load 500 µN

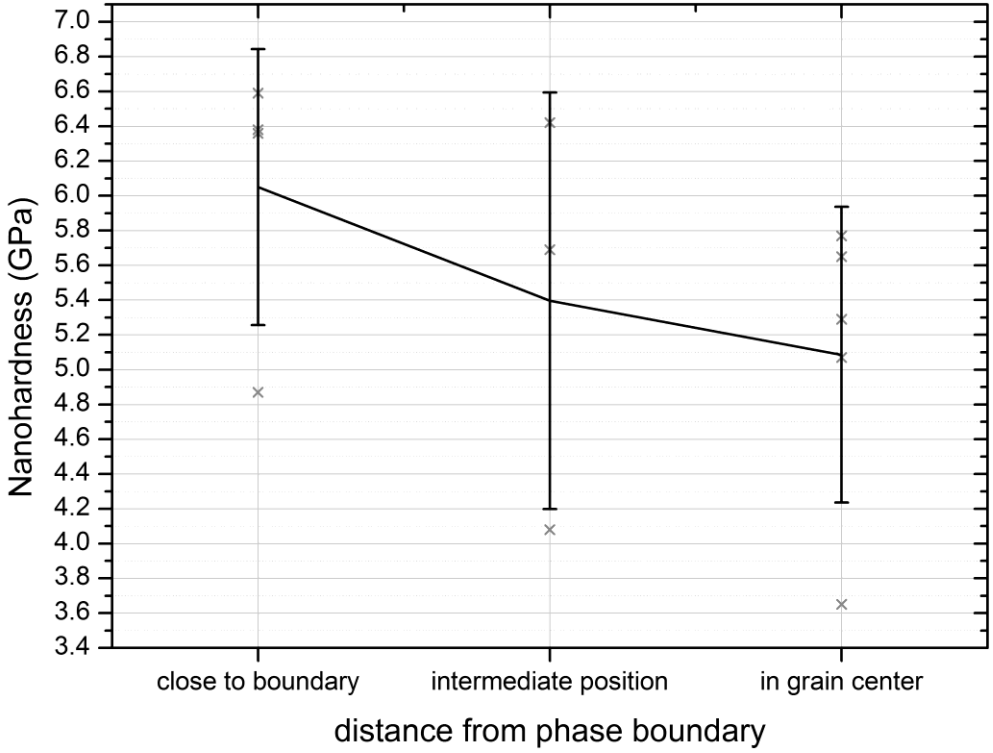

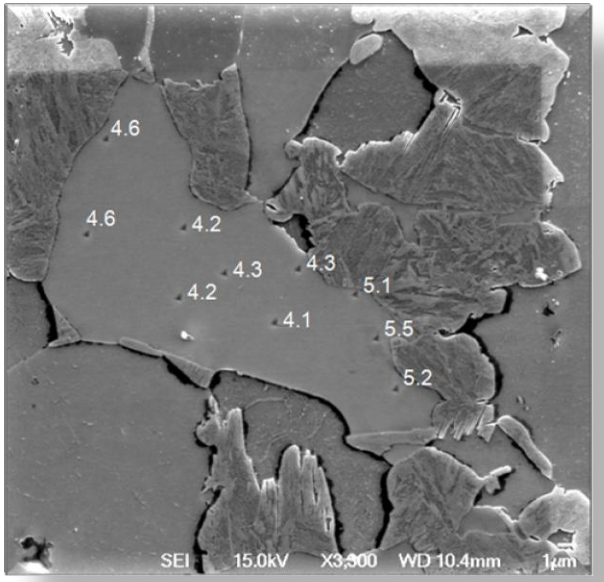

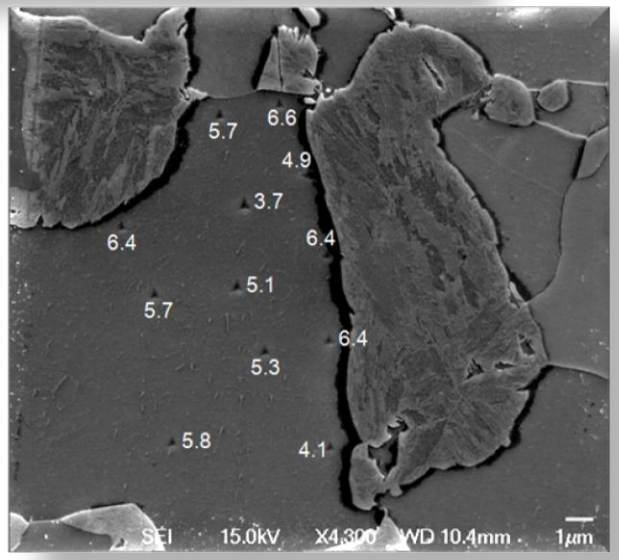

Calcagnotto et al. Mater. Sc. Engin. A 527 (2010) 2738

Overview

- Motivation
- Experiments
- Microstructure and texture evolution
- 3D tomographic analysis of interface regions
- Correlation to DP mechanical properties
- Ultra-fine grained DP
- Conclusions

Conclusions

- Strong through-thickness gradients inherited from hot rolling
- Competition between RX and PT depends strongly on heat treatment conditions
- 3D tomographic analysis of texture and micromechanics
- Correlation of microstructure, texture, orientation gradients and interface strenght

Raabe: Adv. Mater. 14 (2002), Roters et al. Acta Materi.58 (2010)

The Düsseldorf Max-Planck Team

Effect on microstructure

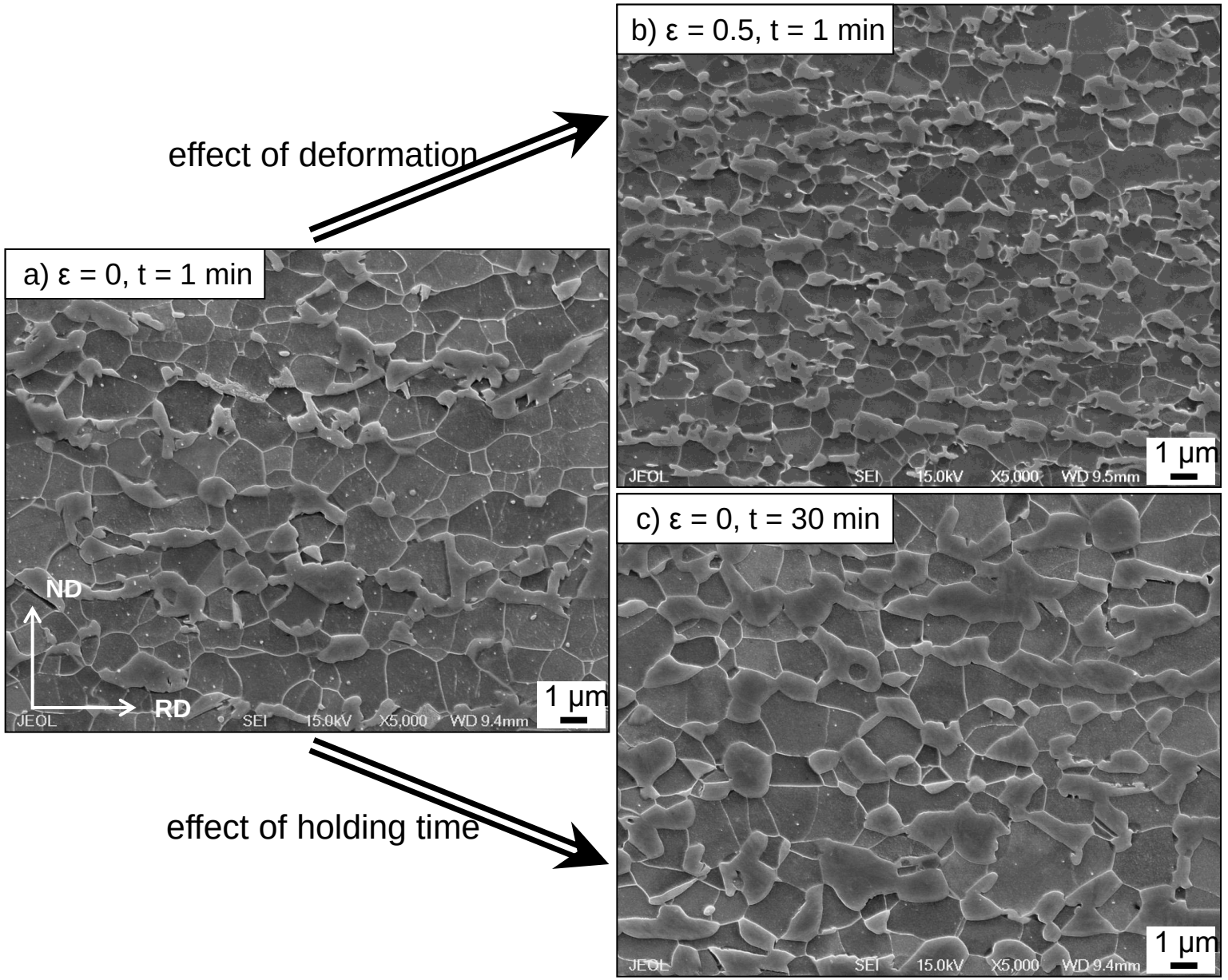

Effect on retained austenite fraction

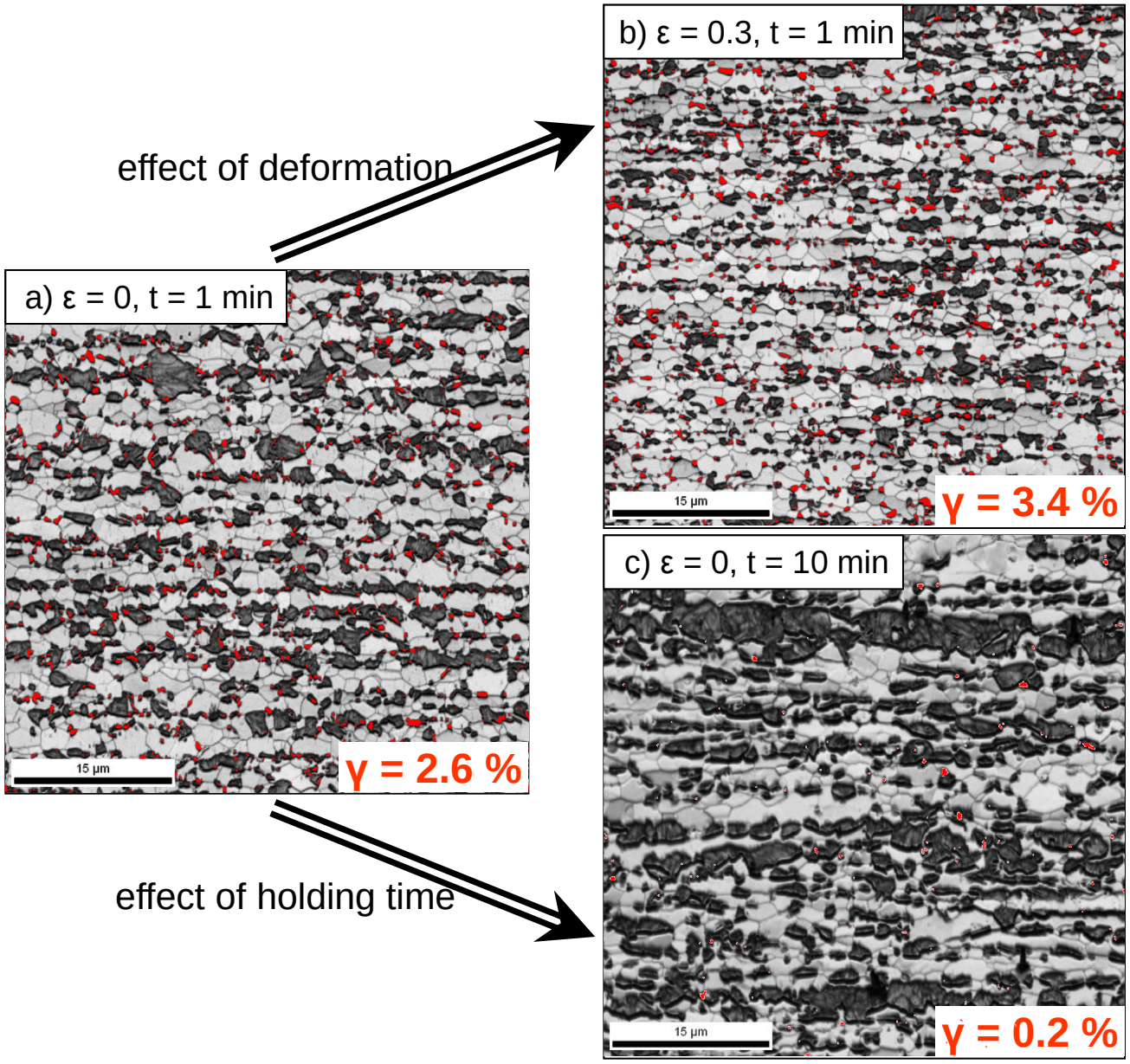

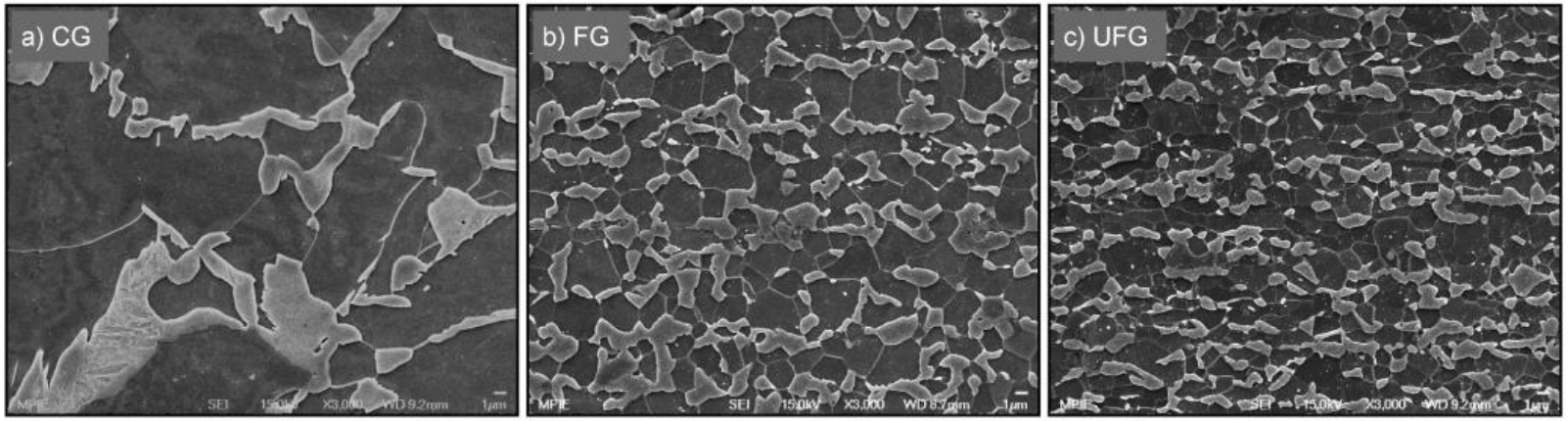

Figure 2: Microstructures used to evaluate the effect of grain refinement on mechanical properites. The a) coarse grained (CG), b) fine grained (FG) and c) ultrafine grained (UFG) material were produced by the processing routes illustrated in Fig. 1 plus inter-critical annealing for 3 min at 730 °C in a salt bath, followed by water quenching.

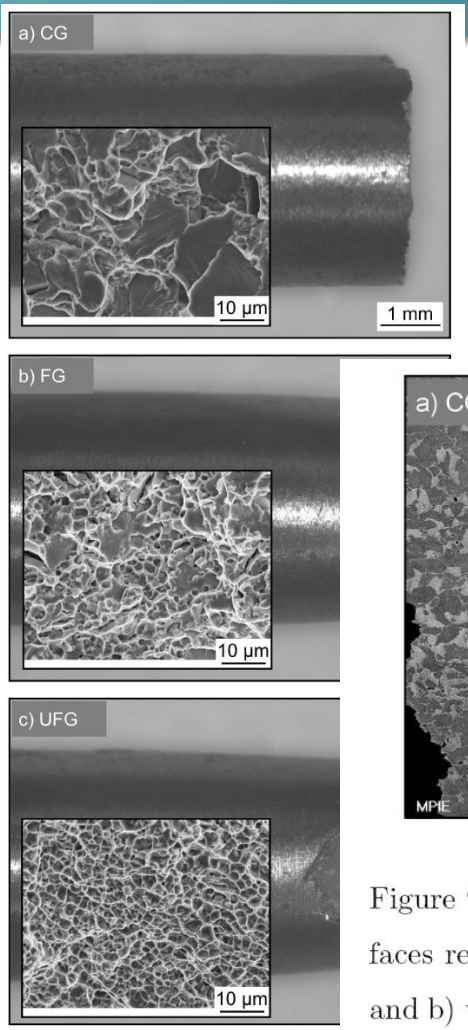

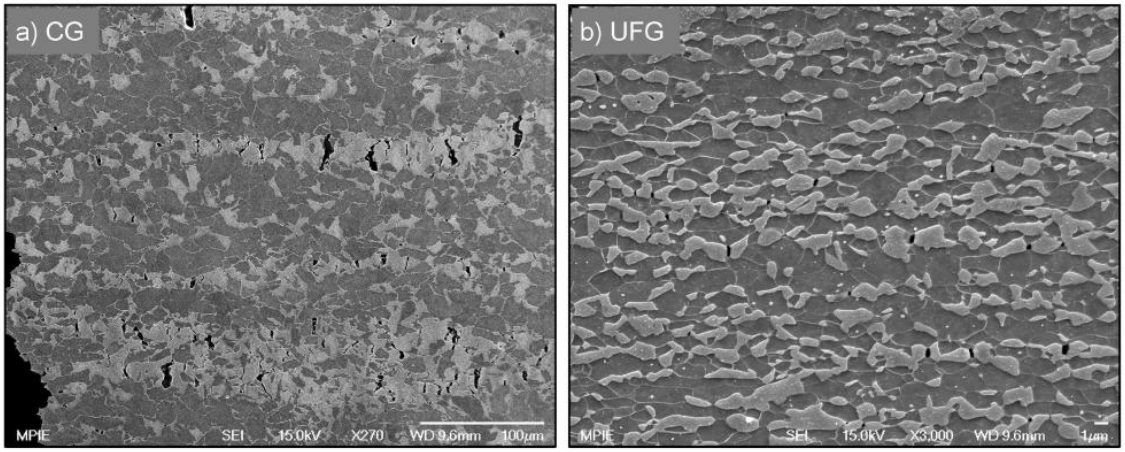

Figure 9: Observation of the planes perpendicular to the fractured tensile specimen surfaces reveal a) martensite cracking as the main fracture mechanism in the CG specimen and b) void nucleation and growth in the UFG specimen. Note the different magnification of the images. The tensile direction is horizontal.

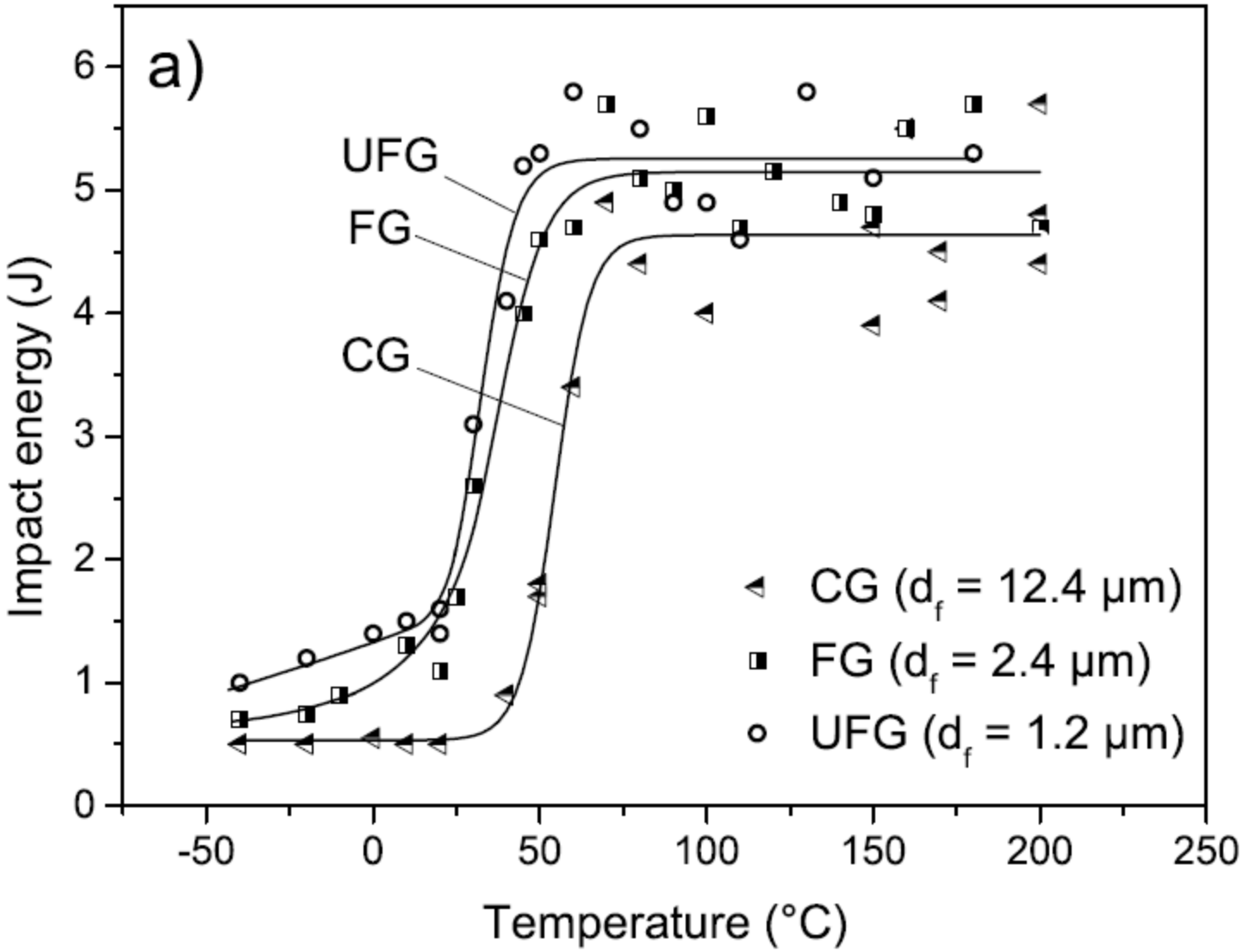
a)
UFG
FG
CG
Impact energy (J)
Temperature (°C)
CG (d_f = 12.4 µm)
FG (d_f = 2.4 µm)
UFG (d_f = 1.2 µm)
0
1
2
3
4
5
6
-50
0
50
100
150
200
250

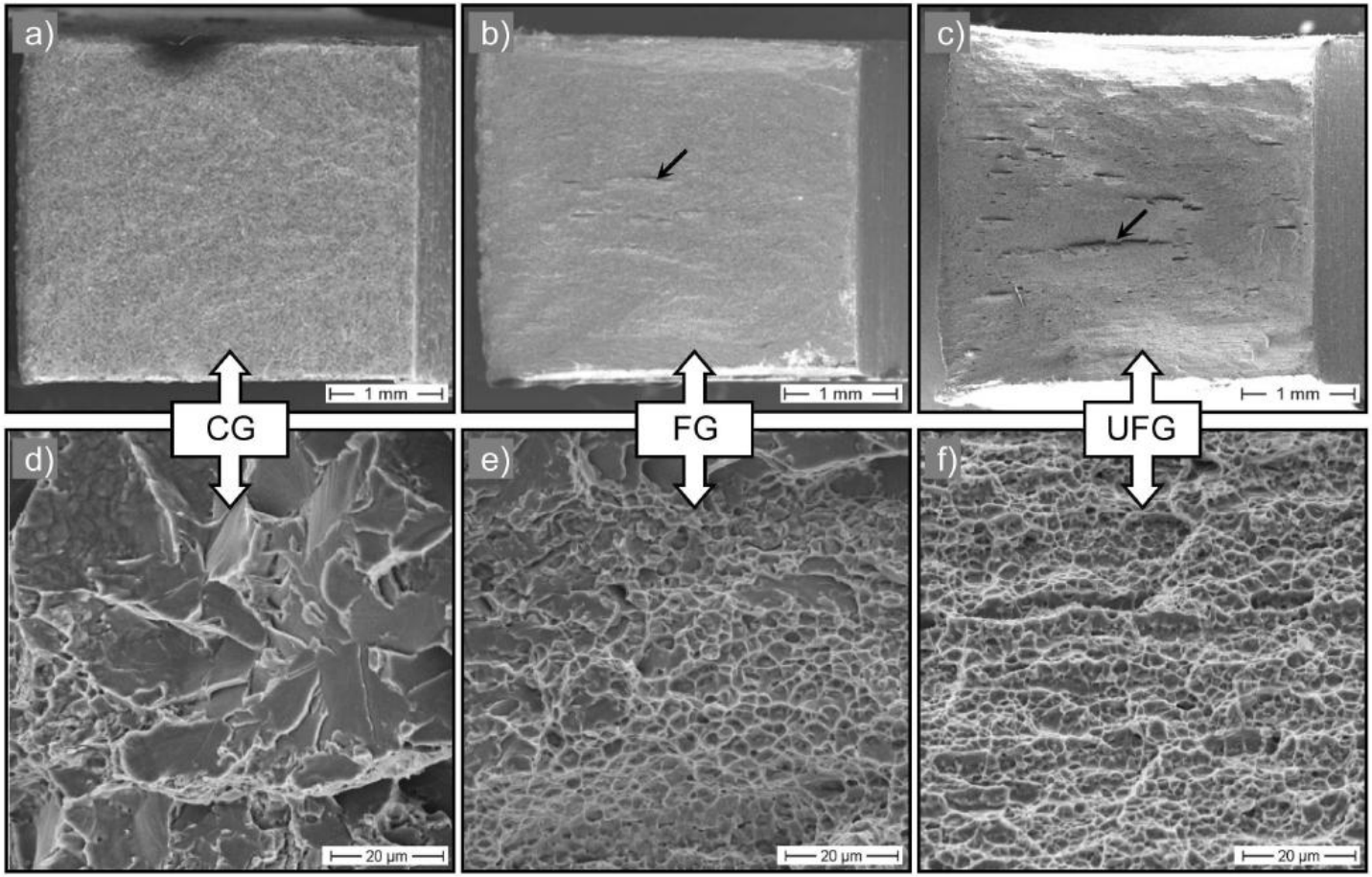

Figure 11: Fracture surfaces of subsize Charpy impact specimen fractured at room temperature. Like in the tensile specimen, grain refinement promotes ductile failure. Some delamination occurs in the FG and the UFG specimen (arrows). Rolling direction is horizontal.